INVESTIGATION OF THE DEPENDENCE OF SHEET RESISTANCE ON THE THICKNESS OF SPIN COATED POLY(3-HEXYLTHIOPHENE) THIN FILMS

OLIVER SIBENGA MUTENDA

APRIL 2024

INVESTIGATION OF THE DEPENDENCE OF SHEET RESISTANCE ON THE THICKNESS OF SPIN COATED POLY(3-HEXYLTHIOPHENE) THIN FILMS

A THESIS SUBMITTED IN PARTIAL FULFILMENT

OF THE REQUIREMENTS FOR THE DEGREE OF

MASTER OF SCIENCE IN PHYSICS

OF

THE UNIVERSITY OF NAMIBIA

BY

OLIVER SIBENGA MUTENDA

200118153

APRIL 2024

SUPERVISOR: DR ZIVAYI CHIGUVARE (UNIVERSITY OF NAMIBIA)

Abstract

Sheet resistance ($R_{\square}$) and thickness of as-cast and post-treated poly(3-hexylthiophene) (P3HT) thin films fabricated on non-conductive glass substrates by the spin coating method, were determined under dark, and illuminated conditions. $R_{\square}$ of P3HT thin films of different thicknesses were compared, to examine the effect of illumination on the $R_{\square}$, and hence on the resistivity of the films. Commercially available P3HT was purchased and dissolved in chloroform ($CHCl_3$). Glass slides were cleaned using detergent, acetone, and alcohol, in an ultrasonic bath, followed by cleaning in distilled water. P3HT thin films were fabricated by spin coating $CHCl_3$ based solutions on cleaned, dry glass substrates, in ambient air. The films were annealed at a controlled temperature, and then the $R_{\square}$ of each thin film was measured, using the in-line four-point probe method. The thicknesses of the thin films were varied by varying the spin speed (ω) of the spin coater. The results showed a correlation between the $R_{\square}$ and the P3HT thin films' thickness. The $R_{\square}$ reduces as the thicknesses of the P3HT thin films increase in the light, and in the dark, for as-cast, and annealed, P3HT thin films. Annealing also reduced the $R_{\square}$ of the P3HT thin films, and $R_{\square}$ showed some reductions when measured in the dark. The four-point probe method can be used to characterise materials.

Keywords: P3HT, sheet resistance, spin coating, thin films, annealing, four-point probe method

List of Conference Proceedings

[1] Mutenda O S, Investigation of the Dependence of Sheet Resistance on the Thickness of Spin Coated Poly(3-hexylthiophene) Thin Films, 2022 *The Annual Research Conference on Agriculture, Engineering and Natural Sciences (ARCAENS - 2022) Online, (November 2022)*

Table of Contents

List of Tables

List of Figures

List of Abbreviations and Acronyms

$CHCl_3$	chloroform
HOMO	highest occupied molecular orbital
ITO	indium tin oxide
LUMO	lowest unoccupied molecular orbital
MM	multimeter
MW	molecular weight
OPV	organic photovoltaic
P3HT	poly(3-hexylthiophene)
PTs	polythiophenes
$R_{\square}$	sheet resistance
rpm	revolution per minute
RR	regio-regular
SVA	solvent vapour annealing

Acknowledgements

Firstly, I would like to thank my supervisor Dr Zivayi Chiguvare for the guidance he has given me in writing this thesis. I would also like to thank my family and friends for the support they have always given to me.

Dedication

I dedicate this thesis work to my family and friends, especially to my Mom and Dad, Mavis & Gilbert, respectively who stood by me through thick and thin, and to the almighty God.

Declarations

I Oliver Sibenga Mutenda hereby declare that this study is my own work and is a true reflection of my research, and that this work, or any part thereof has not been submitted for a degree at any other institution.

Oliver Sibenga Mutenda	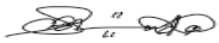	April 2024
Name of Student	**Signature**	**Date**

CHAPTER 1 : INTRODUCTION

This chapter provides an overview of the background of the research, and the research problem and outlines the aims and objectives of the study, the significance of the study as well as the limitations and delimitation of the study.

1.1 Background of the study

In history, civilizations have evolved because of the discovery of new materials, such as during the Stone Age, the Bronze Age, the Iron Age, and the Plastic Age. As the study of material properties progresses, new characteristics of thin films of various materials are currently being identified that have potentially beneficial uses.

Fossil fuels, such as coal, oil, and natural gas, are used to generate the majority of the world's energy and make up around 86 % of all the energy used by the world population [1]. Renewable energy is energy that is derived from resources that can be renewed naturally in a human lifetime. The possibility for high energy conversion efficiency in the capturing of solar energy exists, particularly through photovoltaics. In the laboratory, this technology achieved efficiencies of about 44 % in 2014 [2], but there is still potential for higher values. P3HT is a conductive polymer with numerous uses in electronics, thin films, and organic photovoltaics (OPVs). In the electronics and photovoltaic industries, organic thin films have many advantages over inorganic thin films, including low cost and the potential for roll-to-roll manufacturing [3]. Thorough studies of thin films of organic materials like polythiophenes (PTs), which depend on both material features and production techniques, are required for their widespread use in diodes, transistors, and solar cells.

Utilising centrifugal force, spin coating uses a liquid-vapour interface to deposit a homogeneous film on a solid surface. A liquid is typically poured into the centre of a circular surface that is quickly spun to create homogenous films that range in thickness from 1.0×10^{-8} m–1.0×10^{-5} m. The liquid spreads into a film and covers the surface as a result of the rotation's centrifugal force [4]. The process of heating the active layer after coating to promote solvent evaporation and atom rearrangement in order to change the nanoscale structure is known as thermal annealing [5].

1.2 Statement of the problem

Knowledge of P3HT thin film's electronic properties in relation to fabrication methods, and post-treatment procedures is still limited, and this has slowed down the application of such films outside the research laboratory.

1.3 Aims and Objectives

The study aims to contribute to the knowledge of organic thin films, which have many applications in electronics and photovoltaics, through the following specific objectives:

a) To fabricate thin films of single organic semiconductor material (P3HT), on non-conducting glass substrates, by employing the spin coating method
b) To determine the $R_{\square}$ of as-cast and post-treated P3HT thin films
c) To determine the thicknesses of the as-cast and post-treated P3HT thin films
d) To discuss the relationship between the fabrication method, and the obtained $R_{\square}$, as well as its dependence on the thickness of the film, and
e) To compare the $R_{\square}$ of P3HT thin films in the dark, and under illumination.

1.4 Significance of the study

The study will assist towards the contribution to knowledge towards science in this area. The procedures utilized herein will be utilised in the design and study of thin film devices in the future.

1.5 Limitation of the study

Post-treatment of thin films is limited to thermal annealing. Adjustment to preparation procedures and measurement techniques such as Lasers, Gamma, Infrared spectrometry, and Mass measurement may be limited by the non-availability of equipment such as a reflectometer at UNAM.

1.6 Delimitation of the study

The project is limited to investigating the electrical properties of single P3HT thin films.

1.7 Structure of the thesis

This thesis is divided into five chapters. The first chapter introduces the study and provides a general overview, background of the research problem, problem statement, purpose of the study, objectives of the study, significance of the study and limitation and delimitation of the study. Chapter two presents the literature review and theoretical framework of the study. Chapter three describes the methods used in the study while chapter four presents the results, and analysis of the findings, and

further discusses the findings. Chapter five provides the conclusions drawn and provides the recommendations for further action.

CHAPTER 2 : LITERATURE REVIEW

This chapter reviews published literature on polymers, their applications, and provides examples of recent P3HT and four-point probe method developments. It discusses the problems and potential solutions.

2.1 Polymers

Polymers are a collection of a variety of substances that have the characteristics of being huge molecules produced by chemically joining smaller substances [6]. The words poly, which means many, and mer, which is an acronym for the word monomer, are the sources of the name polymer. The basic building block from which the polymer is constructed is a monomer. A macromolecule is another name for a polymer, suggesting that it is a species with a high molar mass. The phrase "macromolecule" does not always mean that every component along the molecule's backbone is the same. Many synthetic macromolecules are called plastics in modern usage. Polymers are classified in several ways: 1) On the basis of source or origin, 2) On the basis of structure, 3) On the basis of the mode of synthesis, and 4) On the basis of interparticle forces.

1) Classification of polymers on the basis of source or origin

Three categories are used to categorise these polymers: a) Natural polymers b) Synthetic polymers and c) Semi-synthetic polymers.

a) Natural polymers

Natural polymers are those that have been isolated from natural sources, primarily from plants and animals. A few examples are polysaccharides, which are glucose-

based polymers that include starches and cellulose. Proteins are amino acid polymers. They serve as the foundation for animal cells, just like natural protein, wool, and leather do. The polymers of different nucleotides, such as ribonucleic acid and deoxyribonucleic acid, are known as nucleic acids. Latex-derived materials are referred to as natural rubbers. Natural polymers may also be referred to as biopolymers.

b) Synthetic polymers

Synthetic, artificial, or man-made polymers are the names given to polymers that are created in a laboratory. Polystyrene, teflon, polyethene, polyvinyl chloride, synthetic rubber, bakelite, nylon, orlon, polyester, terylene, and others are examples of synthetic polymers. P3HT fits within this category.

c) Semi-synthetic polymers

Semi-synthetic polymers include both synthetically created and naturally occurring polymers, such as acetyl cellulose [7].

2) Classification of polymers on the basis of structure

This classification of polymers is based on their monomeric units and based on their structure, the polymers can be categorised as a) Linear polymers b) Branched chain polymers and c) Cross-linked polymers or Network polymers.

a) Linear polymers

These polymers consist of long, straight chains of monomeric units joined together. To create a densely packed structure, the polymeric chains are piled on top of one another. Such polymers have high densities, high tensile strengths, and high melting temperatures as a result of their close packing. Polyethene, polyester, nylon, and

other common examples of these sorts of polymers are available. Figure 2-1 below shows the linear chain of polymers.

Figure 2-1: Linear chain [7].

b) Branched chain polymers

The monomeric units of this kind of polymer are joined together to form long chains that are also referred to as the main chain. The side chains that make up branches are of various lengths. As a result of their irregular packing, branched-chain polymers have lower densities, tensile strengths, and melting temperatures than linear polymers. Common examples of these categories are glycogen and amylopectin. Figure 2-2 below shows the branched chain of polymer.

Figure 2-2: Branched chain [7].

c) Cross-linked polymers or Network polymers

The monomeric molecules in this kind of polymer are joined together to form a three-dimensional network. Cross-links are the term for the involved links. Because of their network structure, cross-linked polymers are tough, rigid, and brittle. Bakelite, melamine, formaldehyde resin, and other common examples fall into this

category. P3HT thin films have this structure of this classification [8]. Figure 2-3 below shows the cross-linked chain of polymer.

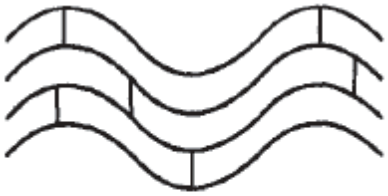

Figure 2-3: Cross-linked chain [7].

3) Classification of polymers on the basis of the mode of synthesis

The different types of polymers in this category include a) Addition polymers and b) Condensation polymers.

a) Addition polymers

Typically, lengthy chains without the elimination of any side product molecules are formed when the monomeric components are repeatedly added. The product created is known as an addition polymer, and the procedure used to create it is known as addition polymerisation. The unsaturated chemicals that make up the monomer units are typically alkenes. As a result, the addition polymer's molecular mass and formula can be seen as an integral multiple of the monomer units.

b) Condensation polymers

In this kind of polymer, the monomers interact with one another by eliminating a molecule like water, ammonia (NH_3) or alcohol, etc. The result is known as a condensation polymer, and that specific reaction or process is known as condensation. The molecular mass of the polymer is not an integral multiple of the monomer units since the process involves the removal of by-product molecules [7].

4) Classification of polymers on the basis of interparticle forces

Van der Waal forces and hydrogen bonds found in the macromolecules play a role in the intermolecular forces that govern the mechanical properties of polymers, including elasticity, tensile strength, toughness, etc. Even though small molecules also exhibit these intermolecular forces, their impact is less pronounced than it is in macromolecules. This is due to these forces combining to produce an effect along the lengthy chains of polymers. Naturally, the effect of intermolecular forces increases with chain length. The polymers are divided into the following four groups based on the strength of the intermolecular forces: i) Elastomers ii) Fibres iii) Thermoplastics, and iv) Thermosetting polymers.

i) Elastomers

The polymer chains in these are supported by the least powerful attractive forces. They are regarded as amorphous polymers because of their great degree of flexibility.

ii) Fibres

These are the polymers that have hydrogen bonds and other strong interparticle interactions. Both their modulus and tensile strength are high.

iii) Thermoplastics

These are the polymers where the forces of attraction between the particles are intermediate between those of fibres and elastomers. By heating the polymers and then allowing them to cool to room temperature, desired shapes can be easily formed from them.

iv) Thermosetting polymers

On heating, these polymers become rigid and infusible. In general, they are created by heating in a mould material with low molecular masses that are semi-fluid. Heating causes the chains to cross-link excessively, creating a three-dimensional

network of linkages as a result of which a hard, non-fusible substance is created [7][9].

Simple low molecular weight (MW) molecules can combine to create complex high-MW ones through a process called polymerisation. Each compound molecule needs to be able to react with at least two additional molecules of the same or a different compound for this procedure, or they need to have a functionality of two. The quantity of a compound's reactive sites determines its functionality [7]. Finding out if polymerisation has taken place by condensation or addition, as was previously discussed, is frequently challenging. As a result, a more logical classification based on the process of monomer unit combination has recently been proposed. Two different types of polymers have been observed, according to this system: a) Chain growth polymers and b) Step growth polymers.

a) Chain growth polymers

Chain growth polymerisation is the process of adding monomer units one at a time through a chain mechanism to the growing chain. By using a little amount of an initiator, such as organic peroxide, an acid, or a base, the monomer unit is transformed into one or more active intermediate species. The intermediate species, which can either be a free radical or an ion depending on the circumstances, combines with additional monomer units to create even larger intermediate species. As a result, intermediate species are added to one after the other using a chain process.

b) Step-growth polymers

Stepwise intermolecular condensation occurs throughout the step-growth polymerisation process through a succession of separate processes. Every reaction includes the loss of a single simple molecule, such as water, NH_3, helium iodide,

alcohol, etc. If the monomer molecules include multiple functional groups, either similar or distinct, this sort of polymerisation will take place. Step growth polymers are the polymers created during step-growth polymerisation [7]. All industrialised cultures have taken use of the desirable qualities of polymers, such as their ease of processing, high strength, and low density, to the point where it is now difficult to envision living without them [10].

2.1.1 Organic Polymers

There are very important materials based on inorganic bonded structures, including silicon-oxygen $(R_2SiO_2)_n$, phosphorus-nitrogen $(P\text{-}N)_n$, boron-nitrogen $(B\text{-}N)_n$, sulphur $(S)_n$, and other chemistries, and these are known as inorganic polymers. The majority of polymers are based on linking molecules that have a carbon-carbon bonded structure. These are the so-called organic polymers [11]. The unpredictable petroleum industry creates organic polymers. Many organic polymers are difficult to incorporate into the biosphere and, when burned, produce highly hazardous by-products. An increasing amount of research is being done on inorganic polymers. In many aspects, inorganic materials may be superior to their organic counterparts due to their vastly different chemical makeup. The polysiloxanes are a notable illustration of this due to their exceptional heat stability. Another is the use of polyphosphazenes in controlled medication delivery systems because of their regulated degradability and their benign degradation products.

The field of ceramics and polymer science can be connected by inorganic polymers. Most of the known inorganic polymer systems are composed of just a handful of elements that belong to the "Main Group" series of the Periodic Table. These

substances are located in IUPAC nomenclature categories III (13), IV (14), V (15), and VI (16) [10].

2.1.1.1 Conductive Polymers

The delocalisation of π-electrons causes certain polymers, known as conducting polymers, to conduct electricity. Such substances may either be semiconductors or exhibit metallic conductivity [12][13]. Conducting polymers like insulating polymers are organic materials. Conducting polymers are highly conjugated, hence also the name conjugated polymers, which gives them their semiconducting or metallic properties. High electrical conductivity is something they can provide, but they don't have the same mechanical characteristics as other commercially available polymers. Advanced dispersion techniques and methods of organic synthesis can be used to fine-tune the electrical characteristics. Conducting polymers synthesised as nanoparticles are of particular interest since they differ greatly from their bulk counterparts in terms of their characteristics. Currently, electrochromic display devices, photovoltaic devices, and biosensors, to name a few, have all been built on the foundation of nanostructures of conductive polymers [14]. Conjugated polymers are insulators in their neutral form; they can be rendered conductive by chemically or electrochemically oxidising (p-doping) or, less frequently, reducing (n-doping) them [15]. Conducting polymers and inorganic semiconductors have very different doping concepts, which cause them to have very different electrical properties. These differences can be summed up as follows:

1) Inorganic semiconductors process few charge carriers, but these carriers have high mobility because of the high crystalline degree and purity presented by these materials. Contrarily, conducting polymers exhibit low mobility due to structural

flaws despite having a high number of charge carriers because of a high doping degree (> 50 %).

2) In metals, a free electron is thought of as a charge carrier and a metal's conductivity is temperature-dependent, rising at lower temperatures. In contrast, an electron or hole is designated as a charge carrier in an inorganic semiconductor, and minion charge carriers (electron or hole) created by n- or p-type doping typically dominate the electrical properties of semiconductors.

The energy gap, which is the difference in energy between the valence band and the conducting band, is used in the band model of charge transport in semiconductors to describe electrical properties. The doping degree is often a function of the conductivity of conducting polymers evaluated at room temperature using the four-point probe method, which demonstrates that conductivity rises as the doping degree increases from insulator to metal through a semiconductor.

3) The chain conformation, morphology, and crystallinity of the final product are all influenced by the polymerisation conditions, which include the concentration of the monomer, dopant, and oxidant, the molar ratio of the dopant and oxidant to the monomer, and the temperature and time of the polymerisation [16]. The fundamental advantage of conductive polymers over other semiconductors is that they are easily processed, particularly through dispersion. One of the most significant representative classes of conjugated polymers, polythiophenes create some of the materials that are both thermally and environmentally stable. Using synthesis, structural flaws can be removed and the amount of overlap along the backbone measured. The creation of new polymers by synthetic chemists, that can be fabricated into novel devices whose physics and chemistry can be thoroughly understood, is a crucial component of both the pioneering work and future work in conjugated polymers [17].

Fundamental properties were found using relatively simple structures in the early years of the concerted and focused studies on conjugated and conductive polymers (1970–1990). Improvements in polymer synthesis, such as the use of cross-coupling processes catalysed by transition metals, enabled the synthesis of polymers with higher structural fidelity and their subsequent characterisation in organic electronic devices in the decade that followed (1990–2000). The ability to test and modify novel structures using the metrics provided by a device application as a source of feedback set the stage for the following decades (2000–2020).

Polymer synthesis is currently in a position where it can take advantage of structural simplicity and seek to create polymer architectures with greater environmental and device stability. With the discovery of more environmentally friendly catalysts, such as those based on copper, the sustainable synthesis of conjugated polymers, such as through direct arylation polymerisation or oxidative direct arylation polymerisation, has a lot of room for growth, enabling the synthesis of a variety of conjugated polymer architectures, including donor-acceptor copolymers [18]. Several general principles should be kept in mind when designing conjugated polymers for various applications, including 1) Side chains to improve solubility and processibility, 2) High MWs, 3) Band gap and absorption behaviour, 4) HOMO and LUMO energy levels, and 5) Appropriate morphology with low barriers. For particular applications, all of these variables must be carefully taken into account because they are interdependent. For instance, sidechains improve the solubility and MW that can be obtained for conjugated polymers, but they also have an impact on their intermolecular interactions through changes in morphology and, consequently, the mobility of charge carriers.

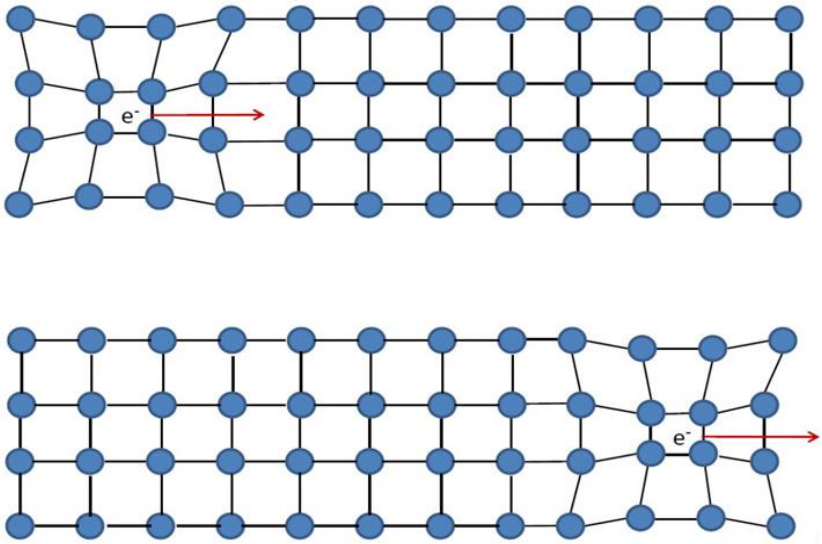

Figure 2-4: A simply depicted polaron. Positive ions are drawn to the electron as it travels through the organic substance. The electron is carried by this lattice deformation [20].

The charge carriers in organic semiconductors are known as polarons because they move through the material not only as positive or negative charge carriers but also as localised deformations. So, in organic semiconductors, terms like positive and negative charge carriers are more common. A light-emitting diode's HOMO and LUMO energy levels are often changed by adjusting the energy band gap to get the desired absorptions, which changes the emitting colour of an organic light emitting diode (OLED). In order to find the right polymers for particular applications, it is vital to properly account for these design principles and balance the guiding concepts [19]. Due to the limited mobility in organic semiconductors, a space charge zone forms at the semiconductor side of a metal-semiconductor contact as electrons are emitted from the metal to the semiconductor in an electric field. The additional injection of electrons from the metal is repelled by this space charge. To move to the semiconductor, the injected electrons must defeat the repelling effects of the space

charge as well as the attractive forces of the metal's lattice (work-function) [20]. Conductive polymers have low dielectric constants [21].

In theory, a property of charge transport for a material can be described by the temperature dependence of the conductivity as determined by the four-point probe method. The logarithmic derivative can be used to express how conductivity varies with temperature:

$$\alpha = \frac{\Delta \ln \sigma}{\Delta \ln T} \tag{2.1}$$

where σ is the conductivity and T is the absolute temperature [16].

2.1.1.1.1 Poly(3-hexylthiophene) (P3HT)

P3HT is a conjugated polymer that is a semiconductor with semi-crystalline qualities. It is one of the frequently investigated polymers for applications in organic electronic devices such as field effect transistors (FETs) and donor material in organic solar cells, and photodiodes [22]. P3HT is one of the most studied organic semiconductor polymers due to its high inherently positive charge carrier mobility, superior solubility and processability [20]. It is stable both in a doped and undoped state. Figure 2-5 a) below illustrates two distinct regio-regulars (RRs) monomers that can be used to insert the 3-hexyl substituent in the thiophene ring into the polymer chain: head-to-tail (HT) and head-to-head (HH). A RR-P3HT, as depicted in figure 2-5 b) below, has only one type of 3-hexylthiophene ($C_{10}H_{16}S$), either HH or HT, as opposed to a regio-random P3HT, which has both HH and HT in a random pattern.

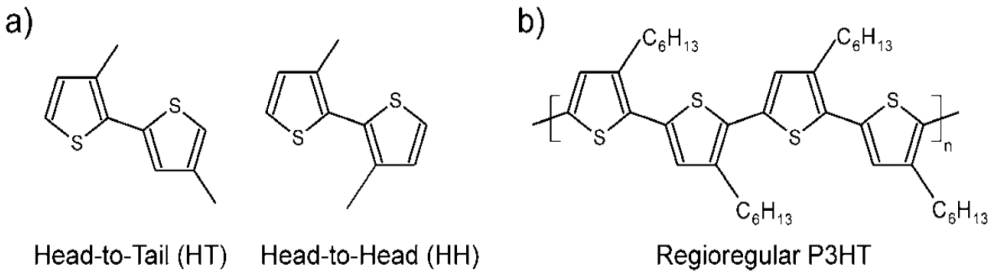

Figure 2-5: a) Two distinct RRs that can be incorporated into polymer chains b) The chemical representation of RR-P3HT [20].

RR-P3HT offers excellent promise as an organic semiconductor in electronics when cast onto thin films due to its propensity to self-assemble into crystallites with ordered structures. Positive charge carrier field-effect mobilities result from this. However, the regio-random P3HT only exhibits positive charge carrier field-effect mobilities because of its twisted chain conformation, poor packing, and low crystallinity. It has also been demonstrated that the MW affects the morphology and charge transport of the RR-P3HT. Additionally, the solvent of choice has a significant impact on the microscopic morphology of the film and, consequently, its mobility [26]. It has been established in the literature that the P3HT oxygen is known to form a charge transfer complex resulting in the p-doping of P3HT. Furthermore, decreased mobilities and higher trap densities have been linked to oxygen-induced P3HT degradation [20]. P3HT has a high absorption coefficient (about 105 cm^{-1}). This makes it very attractive for organic optoelectronic devices. P3HT's mobility is considered low when compared to those of inorganic semiconductors [23]. P3HT is a member of PTs. Thiophenes, sulphur heterocycle, are polymerised to form PTs. The parent PT has the chemical formula $(C_4H_2S)_n$ and is an insoluble coloured solid [24]. Through the 2- and 5-positions, the rings are connected. Alkyl substituents are present at the 3- or 4-position in poly(alkylthiophenes)(s).

Table 2.1: Properties of P3HT.

Full name	Poly(3-hexylthiophene-2,5-diyl)
Synonyms	P3HT
Chemical formula	$(C_4H_2S)_n$
Form	Powder, Brown to Black colour
Melting point	511.45 K
Average MW	54 000–75 000
Highest occupied molecular orbital/Lowest occupied molecular orbital	HOMO = -5.2 eV LUMO = -3.2 eV
Solubility	$CHCl_3$, chlorobenzene (C_6H_5Cl)
Classification/Family	PTs, Organic semiconducting materials, Low band gap polymers, Polymer donors, OPVs, Polymer solar cells, organic light-emitting diodes, organic field-effect transistors (OFETs)
Semiconductor properties	P-type (mobility = 10^{-4}–10^{-1} cm^2 V^{-1} s^{-1})

They are coloured solids as well; however, they usually dissolve in organic solvents. If PTs are oxidised, they become conductive. The delocalisation of π-electrons along the polymer backbone is what causes the electrical conductivity. The conjugated polymers' optical characteristics react to environmental cues, changing colour dramatically in response to variations in solvent, temperature, applied potential, and molecular binding. Conjugated polymers are appealing as sensors because they can produce a variety of optical and electrical responses. Changes in colour and conductivity are caused by the same mechanism, twisting of the polymer backbone and interrupting conjugation. Table 2.1 below displays the properties of P3HT, these are the properties of P3HT used in the experiments of this project.

Figure 2-6 below shows the structural formula of P3HT. It is a benzene ring with sulphur in it.

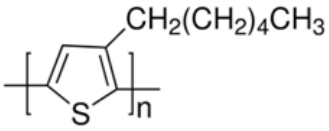

Figure 2-6: P3HT's molecular structure [25].

The properties of RR-P3HT make it a preferred reference material for both fundamental and applied research in organic electronics, physics, and chemistry. These properties include partial air stability. P3HT is frequently accepted as the standard by which any new p-type or donor conjugated molecule should be examined and assessed because it is one of the extensively researched organic semiconductors.

3-Alkylthiophene can be polymerised using a variety of chemical synthesis techniques, such as the Rieke, McCullough, and Grignard metathesis procedures. These methods mentioned above differ in that they produce polymers with low MW and high regioregularity content. However, these procedures necessitate more than one phase of the reaction and unique synthesis conditions, such as a temperature maintained at lower than -5 °C or higher than 60 °C.

Despite not producing high regioregularity polymers, the chemical synthesis with ferric chloride ($FeCl_3$) is perhaps the most popular due to its ease of use and potential for large-scale use. $CHCl_3$ is almost always used as a solvent in polymerisations' reactions of poly(3-alkylthiophene) by chemical oxidation with $FeCl_3$. When compared to other approaches, this polymerisation results in polymers with a high MW and a regioregularity of roughly 70–80 %. Since the same regioregularity is maintained, polymers with lower MW present stronger electron conduction in some applications, such as those that need electron conduction. In some studies, the decline in crystallinity of these polymers is blamed for the decrease in electron conduction that occurred along with an increase in MW [26].

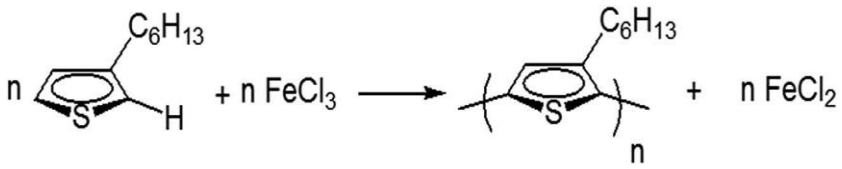

Figure 2-7: Oxidative coupling to synthesise P3HT in the presence of $FeCl_3$ [27].

The ratio of monomer to $FeCl_3$ is always preserved at 1:4 when polymerising P3HT by oxidative coupling of $C_{10}H_{16}S$ (monomer) in the presence of $FeCl_3$. A reaction flask containing anhydrous $FeCl_3$ suspended in $CHCl_3$ is typically flushed with nitrogen before being sealed. In general, the initial monomer concentration in $CHCl_3$ is maintained at 0.05 M. Using a syringe, the $C_{10}H_{16}S$ solution is gradually injected into the $FeCl_3$ suspension. Under a nitrogen environment, polymerisations are conducted at room temperature for 86 400 s. To precipitate the polymer, the resulting black reaction mixture is added to methanol (CH_3OH). Precipitates are then washed with CH_3OH using a Soxhlet extractor. Using the same extractor, the polymers are extracted with $CHCl_3$. After the solvent has evaporated at room temperature, the polymer is collected. The reaction equation between $C_{10}H_{16}S$ and $FeCl_3$ to produce P3HT is shown in figure 2-7 above.

Despite significant differences in MW between polymers made with dichloromethane (CH_2Cl_2) and $CHCl_3$, these polymers exhibit no significant differences in regioregularity or conjugation length [26]. In the past, it has been discovered that mobility is favourably connected with growing region-regularity, long drying time (obtained using a solvent with a high boiling point), reduction of the surface energy, and MW greater than MW = 50.0.

P3HT has drawbacks. For example, because film formation is typically accomplished through a wet-coating process, which is also constrained by the wetting characteristics of the P3HT solution with the substrate materials, the light

transmittance is typically not enhanced up to 90 % and the surface morphology of fabricated P3HT films is generally poor [28]. When the ITO/P3HT/Al device is biased with a high potential on Al and the temperature is below 240.0 K, the current flow across the device is constrained by hole injection at the Al/P3HT interfaces, according to the current-voltage characteristics of the ITO/P3HT/Al devices. Above this temperature, the characteristics are governed by the bulk transport properties. For the reverse bias, the ITO/P3HT contact does not limit the current; instead, it is limited by a space charge that builds due to the low charge carrier mobility in the polymer [29].

There is an increase in the Hall mobility and conductivity of P3HT and blended films after a short time of annealing, especially in the case of the blends [30]. Thermal annealing of P3HT films occurs via two stages, the first of which is impurity dedoping leading to some reduction of conductivity, and the second of which involves thermal motion of polymer chains resulting in reordering and, possibly, crystallisation, eventually ending up with an increase in conductivity [31]. For thin films, the melting behaviour is different because the crystals keep pinned at the film/substrate contact up to the melting temperature. Due to the interface contact, the melting temperature is projected to alter as a function of film thickness. Temperature treatment is crucial for the optimisation of P3HT films, and that thickness dependency is critical for understanding the structural characteristics of thin layers [32].

2.2 Thin Films

A layer of material with a thickness of 9.9×10^{-7} m or less is considered a thin film. A layer of a substance that is thick is one that is between 1.0×10^{-6} m–1.0×10^{-5} m thick. A stack of thin films is called a multilayer.

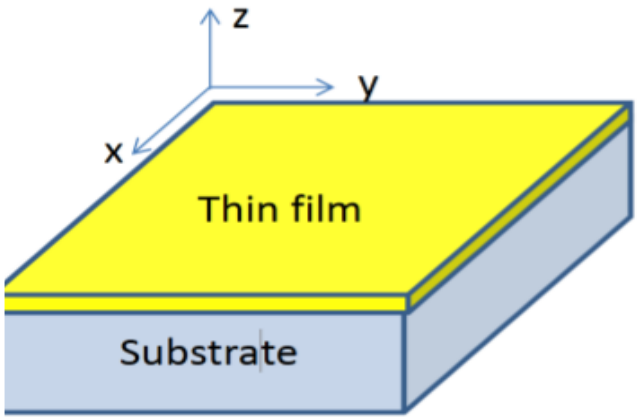

Figure 2-8: A thin film layer on top of a substrate [33].

Layers of polymer material with a thickness of 9.9×10^{-7} m or less are referred to as polymer thin films. Thin film technology is founded on three foundations: 1) Fabrications 2) Characterisation and 3) Applications.

1) The manufacture of thin films is carried out by employing standard physical and chemical vapour deposition techniques and modifications through, ion assistance and laser ablation.

2) Characterisation of thin films can be based on film thickness, structure, and chemical composition. The characterisation of a thin film can be substantially different from that of bulk material because thin films, as two-dimensional systems, have a large surface-to-volume ratio. In addition, thin films differ from the corresponding bulk materials in terms of shape, physical structure, and chemical

composition. Another thing is that thin films' characteristics can be significantly influenced by the surface and/or interface properties of the substrate due to surface mobility, stress effects from thermal expansion mismatch, and other factors. As a result, there exist specialised techniques for the examination of surface/interface shape and composition as well as nanoscale crystallographic and electrical structure.

3) Applications: Electronics, coatings, and photovoltaics are some examples of thin film application categories [34].

Thin films are used in semiconductors, mirrors, lens coatings, and many other applications, and their significance in physics and engineering has grown over time. Applications for optical electronics, communications, a variety of coatings, energy generation, and energy conservation are all found in the industry [35]. Thin films can withstand extremely high residual stresses because of their frequently high yield strengths. Through plastic deformation, thin film fracture, or interfacial delamination, this residual stress might be released later either during processing or during device operation. For characterising thin films, elastic and plastic characteristics are both crucial. Tensile testing of freestanding films and the microbeam cantilever deflection technique can both be used to measure the mechanical properties of thin films, but nanoindentation is the most straightforward method because no special sample preparation is needed, and tests can be carried out quickly and cheaply [36].

2.3 Fabrication of Thin Films

The technique of placing a thin film of material onto a substrate or previously placed layers is known as thin film fabrication. Deposition methods for thin films can be broadly divided into five categories: plating, oxidation, wet processing, physical

vapour deposition, and chemical vapour deposition [36]. The electrical characteristics of thin films are directly impacted by different processing methods used in semiconductor manufacture. Monitoring thin films during fabrication requires non-destructive, quick, accurate measurements that are sensitive to changes in thin film electrical characteristics. This allows for in-line process control, optimisation, and early detection of process excursions [37]. The solution processing methods presented in figure 2-9 below are widely used in laboratories, and they are mostly called wet processing.

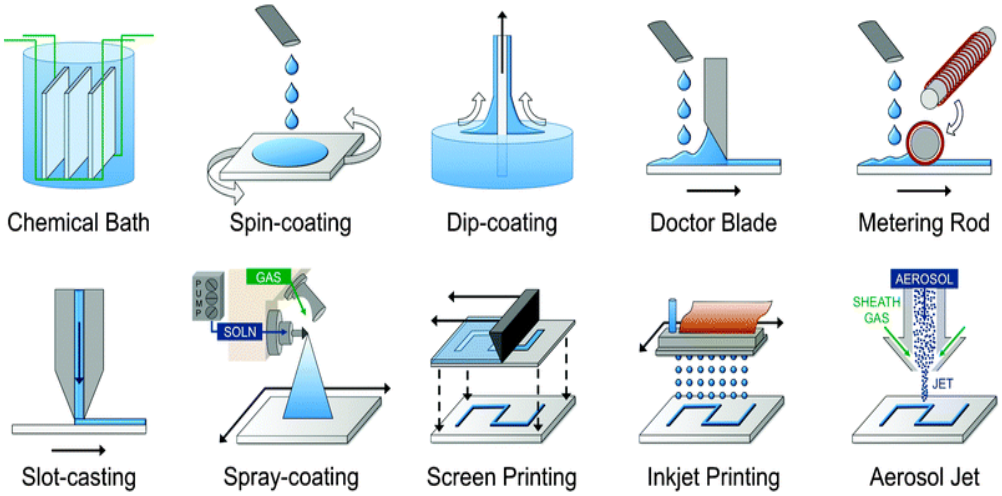

Figure 2-9: Methods for solution processing to fabricate thin films [38].

According to Roncaselli et al. [39], it is well known that changing the solvents causes changes in the morphology and, as a result, the organisation of the morphology of the material, which affects the conductivity. P3HT's solubility would cause the chain to take on various conformations, resulting in crystallinity with a range of sizes. P3HT's chains "stretch" due to its high solubility in $CHCl_3$, increasing the mobility of charge carriers. While xylene's solubility is lower, it would cause the chains to compress, reducing charge carrier mobility and molecular aggregation

during the creation of films. The solvent may improve the efficiency of the solar cell by enhancing photocurrent, enabling charge carrier transport, and establishing percolation channels for carriers. The conductivity value for fully pure P3HT solubilised with $CHCl_3$ is 4.80 x 10^{-6} S m^{-1} [39].

When P3HT is ultrasonically processed, it is most likely to cause the $CHCl_3$ polymer chains to aggregate. During the ultrasonication, the polymer-polymer interactions become more favourable than the polymer-solvent interactions, especially in chlorinated solvents (i.e., $CHCl_3$, C_6H_5Cl and trichlorobenzene ($C_6H_3Cl_3$)). After the spin coating and annealing procedures, polymer films produce a planar and rigid chain conformation with a higher degree of intra-chain contact in comparison with the P3HT film without the ultrasonication step. It can be demonstrated that ultrasonication of a P3HT solution in $CHCl_3$ causes significant variations in the film that remain following spin coating and thermal annealing. Even while the film's general shape remains the same, it has a different λ_{max} of 5.20 × 10^{-7} m and shows lower oxidation start voltages at the longest ultrasonication period ever recorded. By atomic force microscopy imaging, it is discovered that the creation of regionally well-organised aggregated polymer clusters is responsible for the expansion of bigger domain sizes and the alterations in electrochromic behaviour. The film from the solution that has been ultrasonically treated for 480 s shows the lowest threshold for absorbance change and the greatest stability while repeatedly applying 1.0 V/0 V cycles.

Although the precise process is still being researched, ultrasonicating the polymer solution before spin coating serves to improve the behaviour of the device in all measurable characteristics with no clear drawback [40]. In P3HT thin films embedded with preformed crystalline P3HT nanowires, the effects of solvent vapour

annealing (SVA) on the molecular ordering, morphologies, and charge transport properties were thoroughly investigated. SVA with $CHCl_3$ was discovered to dramatically impact the structural and morphological alterations, and therefore on the charge transport characteristics, of the P3HT-nanowires-embedded P3HT films.

With increasing annealing time, the density of crystalline P3HT nanowires was enhanced inside the resultant films, and also intra and intermolecular interactions of the corresponding films were significantly improved. As a result, the P3HT-nanowires-embedded P3HT films annealed with $CHCl_3$ vapour for 1 200 s resulted in a maximised charge carrier mobility of ~ 0.102 $cm^2 V^{-1} s^{-1}$, which is higher than that of pristine P3HT films by 4.4-fold (~ 0.023 $cm^2 V^{-1} s^{-1}$) [41]. Ultrasonication of the polymer solution regulated and increased the intra-chain interaction of the resultant polymer film on an ITO substrate. By using this technique, the polymer film was able to change colours at 0.2 V less voltage than an untreated film while maintaining good stability and a quick response switching time of 1–2 s. It has been shown that using this technique makes it simple to reduce the applied voltage while also enhancing the stability of the electrochromic RR-P3HT film [40].

Abdellah et al. [42] conducted a comparative analysis of OFETs made of P3HT and related their performance to how their morphology depended on the consistency of the solutions employed and the deposition method. Regardless of the deposition procedure, charge carrier mobilities in samples made using fresh solutions have been reported to be in the order of 10^{-4} $cm^2 V^{-1} s^{-1}$. The carrier mobilities in the devices rise as a result of the use of aged solutions at least one order of magnitude or more. The mobilities in spray-coated OFETs were discovered to be of the order of 10^{-3} $cm^2 V^{-1} s^{-1}$, which is on par with the values reported by Abdellah et al. [42] and a factor of one lower than those in the P3HT FETs fabricated by Chan et al. [43] using an

optimised fabrication technique. Even greater mobilities are displayed in spin coated P3HT thin films that were formed utilising aged solutions, especially in samples where some nanofibres were oriented parallel to the channel length [44].

2.3.1 Spin Coating

Applying uniform thin films to flat substrates could be done through the process of spin coating. In a typical procedure, a small puddle of fluid resin is placed in the centre of a substrate, and the substrate is then spun rapidly (typically at a speed of about 3 000 rpm) [45]. A thin resin film will form on the surface due to the resin spreading to, and eventually leaving the substrate's edge due to centrifugal force. Final film thickness and other attributes will rely on the nature of the resin (viscosity, drying rate, per cent solids, surface tension, etc.) and the parameters chosen for the spin process. The properties of coated films are defined in terms of final rotational speed, acceleration, and fume exhaust [45][46]. The main advantages of spin coating are: 1) It is suitable for both research and quick prototyping because of how simple and relatively simple it is to set up a process and because it can produce thin, homogeneous coatings at a range of thicknesses; 2) The capacity to dry materials quickly (because of the strong airflow) results in good consistency at both macro- and nanoscales and frequently eliminates the need for post-deposition heat treatment; 3) In comparison to other techniques, many of which demand both more expensive machinery and high-energy processes, spin coating is an inexpensive way to batch process individual substrates.

Spin coating's main drawback is that it is a batch (single substrate) process by nature, which results in a lower throughput than roll-to-roll processes like slot-die coating.

The amount of material actually used in a spin coating process is also typically very small (at 10 % or less), with the remainder being wasted, and thrown off to the side. In research settings, this is typically not a problem, but in large-scale manufacturing, it is wasteful. Some nanotechnologies, like small molecule OFETs, which need time to self-assemble and/or crystallise, may perform worse due to the fast-drying times [47]. Figure 2-10 below shows the four key steps of spin coating which are: a) deposition, b) spin-up, c) spin-off, and d) evaporation.

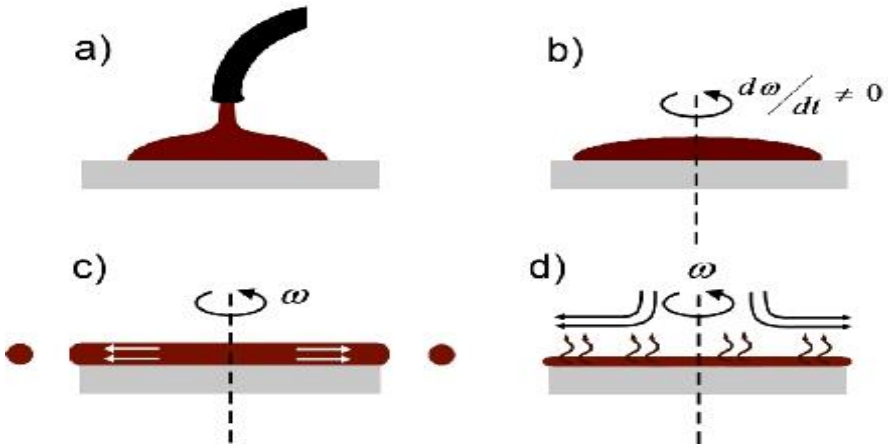

Figure 2-10: The multiple "stages" of spin coating a) Dispensation b) Acceleration c) Flow dominated d) Evaporation dominated [46].

The work of Emslie, Bonner, and Peck (EBP) [48] provides a thorough description of the physics of fluid flow on a spinning substrate. It is expected that the fluid layer is sufficiently thin to ensure that the viscous drag caused by the fluid precisely balances the radial rotational forces. The differential equation (2.2) mathematically expresses the force balance:

$$-\eta \frac{\partial^2 v}{\partial z^2} = \rho\omega^2 r \qquad (2.2)$$

where r is the radius under consideration, v measures the radial velocity component, ρ is the fluid density, ω is the rotation rate/spin speed, z is a vertical height dimension, and η represents the fluid's viscosity. It should be noted that the gradient in the shear created by the velocity vs depth profile is calculated on the left-hand side and that this must precisely balance the forces of rotation experienced by the same volume element. The fluid velocity profile with depth was determined to have the following expression by EBP after solving equation (2.2) with the proper boundary conditions:

$$v = \frac{1}{\eta}\rho\omega^2 r\left[hz - \frac{z^2}{2}\right] \tag{2.3}$$

where h is the instantaneous fluid thickness and z varies from 0 to h. EBP were able to derive a function for the fluid depth against time and calculate the overall fluid thinning rate by integrating. It was discovered that their thinning rate was:

$$\frac{dh}{dt} = -2Kh^3 \tag{2.4}$$

where K is a flow constant and is defined as follows:

$$K = \frac{\rho\omega^2}{3\eta} \tag{2.5}$$

The fact that volatile solvents are typically included in coating solutions' recipes and that their evaporation aids in fluid thinning was overlooked in EBP's treatment. Meyerhofer [49] introduced this crucial element into the equation. It was realised that vapour diffusion via the aerodynamic boundary layer above the wafer surface determined the evaporation rate rather than the fluid's physical thickness. This evaporation contribution to thinning was therefore:

$$\frac{dh}{dt} = -e \tag{2.6}$$

where *e* is a function of ω because the vapour boundary layer changes thickness as the rotation rate changes [49]. e is therefore determined to comply with:

$$e = C\sqrt{\omega} \tag{2.7}$$

where C is a proportionality constant that depends on whether airflow above the surface is laminar or turbulent as well as the diffusivity of solvent molecules in the air (since it is essentially constrained by the diffusion of the evaporating molecules through the aerodynamic boundary layer above the surface of the wafer during spinning). Previously, a laser interferometry approach was merely used to calculate C experimentally [50]. This technique has been called "optospinography" by others who have used laser interference effects [51]. Therefore, under most actual spin coating conditions, both processes will be active at the same time and throughout the operation. The thinning rate differential equation that arises from this is as follows:

$$\frac{dh}{dt} = -2Kh^3 - e \tag{2.8}$$

Fitting interferometry data to derive the e and K constants for specific coating solutions was done using equation (2.8) [50].

By allowing for an estimation of the final film thickness in terms of the important physical constants, Meyerhofer [49] realised that the evaporation term is fluid thickness independent, whereas the flow term has a cubed dependence on h. This suggested that at large thickness values, the flow would take over, decreasing the thickness until it was negligible in relation to the rate of evaporation. A "cross-over" point, was where the two contributions would be equal. Then, the assumption was made that the film would essentially form by drying in place after the cross-over point. (which is the period when evaporation predominates). Using this method, the

calculated final coating thickness, h_f, in terms of the important solution parameters is as follows:

$$h_f = x\left(\frac{e}{2(1-x)}K\right)^{\frac{1}{3}} \tag{2.9}$$

where x is the fractional solids content of the solution (i.e., what would remain once the solvents are totally removed by evaporation or baking), and e and K are the evaporation and flow constants, as previously described. Equation (2.9) then combines e and K's intrinsic dependencies on ω to predict that the ultimate coating thickness will fluctuate with the ω's inverse square root:

$$h_f \propto \omega^{-\frac{1}{2}} \tag{2.10}$$

Numerous experiments have detected this ω exponent of $-\frac{1}{2}$ [49] however, certain reports of values that vary slightly from $-\frac{1}{2}$ have also been made [49]. Previous studies [52] ascribed variations from a value of $-\frac{1}{2}$ to the presence of more viscous liquids or viscosity alterations during spinning. In reality, according to EBP's thickness solution [48] a ω exponent of -1 would be expected in the absence of evaporation. However, some experimental work has produced smaller magnitude exponents, and these discrepancies cannot be explained by either model [49].

The above implies that the thickness of a film will be halved when spun at four times the speed. Equation (2.10) can also be used to calculate a spin curve, as demonstrated in figure 2-11 below.

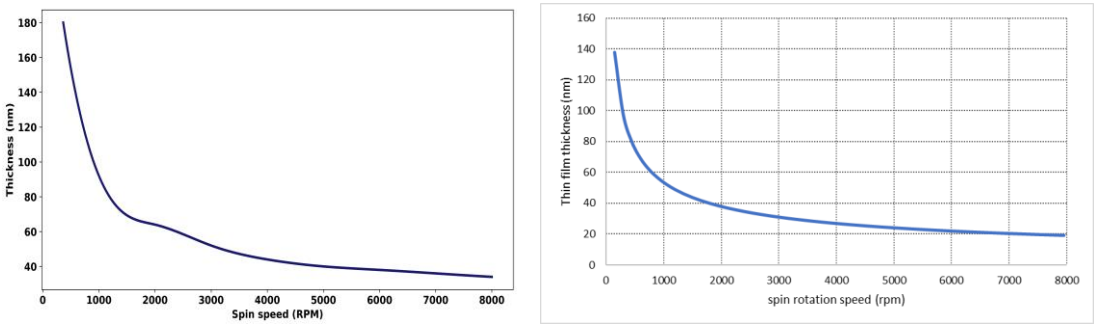

Figure 2-11: Spin curve for a solution (Left side) [47], Reproduced with a fitted proportionality constant of 1670 (Right side).

2.4 Determination of the Thickness of Thin Films

The widely used techniques in thin film thickness measurement are as follows: stylus profilometry, interferometry, ellipsometry, spectrophotometric measurements and x-ray microanalysis [53]. Figure 2-12 below displays the plotted solution concentration against the film thickness graph. Conjugated oligomer (CO) 1,4-bis(9-ethyl-3-carbazo-vinylene)-9,9-dihexyl-fluorene (BECV-DHF) thin films that were cast onto a quartz substrate using a spin coating process. To create thin films of various thicknesses, CO BECV-DHF was dissolved in $CHCl_3$ at various concentrations [54]. In general, increasing the solution concentration results in a thicker film. The higher fluid viscosity is the cause for this [55].

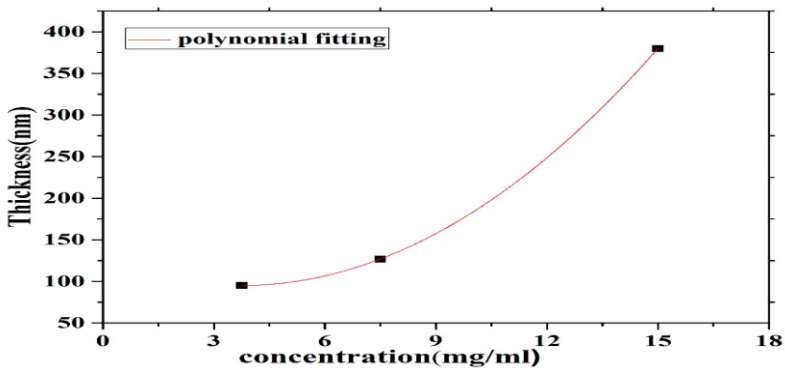

Figure 2-12: Film thickness vs the solution concentration for CO BEVC-DHF deposited by spin coating at 2 000 rpm [54].

Figure 2-13 below indicates that the thin film thickness decreases as the ω increases. Additionally, it demonstrates that when polystyrene (PS) polymer thin films are spun coated and fabricated in $CHCl_3$ as the solvent, the higher the solution concentration the thicker the thin films become.

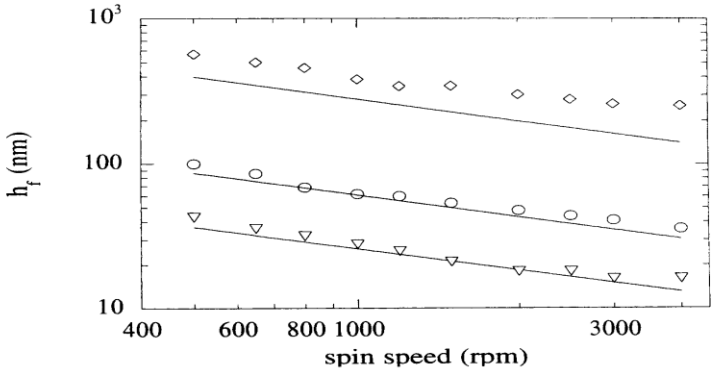

Figure 2-13: The relationship between ω and the initial polymer solution concentration for three different concentrations of polystyrene (PS) in $CHCl_3$: (▽) 0.25 wt % PS, (○) 0.5 wt % PS, and (◊) 2 wt % PS. Solid lines represent predictions of $h_f = (1 - x_1^o)h_\omega$, where h_ω is the wet thin film thickness at which the thin film is anticipated to become immobile and x_1^o is the initial solvent mass percentage in the coating solution [56].

The thickness of the film can also be determined from the mass change of the substrate (before and after the coating procedure) using a high precision weight balance. The thickness of the film h_f can be calculated by using the formula:

$$h_f = \left(\Delta m \cdot \rho_s\right) / \left(m_s \cdot \rho_f\right) \times d_s \qquad (2.11)$$

where ρ_s, d_s, and m_s are the density, thickness, and mass of uncoated substrate respectively. ρ_f the density of the film deposited [35].

The problem that can be experienced with the above method when utilising it on annealed thin films is that thin films come out from the heating oven weighing less than when they went in. This might be due to outgassing effects [57]. At first look, measuring the weight of the film deposit seems to be a simple and direct technique to determine the film thickness h_f using equation (2.11). Precision mass balances rather than interferometers or stylus instruments are more frequently employed in poorly equipped laboratories, where this straightforward method has been used frequently. Because the film density cannot be known with confidence, the values of h_f thus derived are not accurate. The film packing factor P, which measures the void content, might be quite low, for example, P = 0.75 for porous deposits, which is the cause of this. Equation (2.11) would obviously be understated if handbook bulk values of ρ were utilised. The effective deposit area will also be greater than the estimated projected area when the substrate has a lot of relief, such as roughness, cleavage steps, patterned topography, etc. The film thickness in this instance can be overstated.

Using the gravimetric method approach is troublesome for ultrathin films with an island structure. Even though gravimetric methods have drawbacks, extremely fine and cutting-edge microbalances have been developed and are frequently used to track film thickness as it is deposited. Designs for microbalances have utilised ideas like the torsion of a wire, the elongation of a thin quartz-fibre helix, or the deflection of a pivot-mounted beam. Sensitive optical and, more frequently, electromechanical transducers and compensators have been used to enable the detection of $\cong 1.0\times10^{-8}$ g in null measurements. Deposits that are fractions of a monolayer thick can be measured by using very light, large-area substrates. For low density materials (such as silicon dioxide) and high-density metals (such as platinum), typical equivalent

film thicknesses of less than 1.0×10^{-9} m–1.0×10^{-10} m, respectively, are visible. Microbalances composed almost entirely of quartz can operate in an ultrahigh vacuum because they can be degassed at high temperatures. The use of quartz crystal oscillators is the most significant gravimetric method. This method is practically always used to measure the thickness of physical vapour-deposited films in real time [35].

2.5 Sheet Resistance, $R_{\square}$

$R_{\square}$ sometimes termed surface resistivity is the resistance of a thin square film/sheet of material. The units for $R_{\square}$ are **Ω**. The units **Ω** per square, or **Ω**/□, are commonly used. The $R_{\square}$ is numerically equal to the measured resistance of a square piece of the material. $R_{\square}$ is independent of the size of the square measured, and it is not necessary to know the film thickness to measure $R_{\square}$.

Consider the resistance of a square rod with cross-sectional area = A, length = L and width = W, is given by

$$R = \rho \frac{L}{A} = \rho \frac{L}{Wt} \tag{2.12}$$

where t is the thickness of the rod, ρ is the bulk resistivity of the material rod. If its geometry is a square, then L = W therefore $L/W = 1$ implying that

$$R = \rho \cdot \frac{1}{t} \tag{2.13}$$

Since

$$R_{\square} = \frac{\rho}{t} \tag{2.14}$$

$$\Rightarrow \qquad R = R_{\square} \cdot \frac{L}{w} \tag{2.15}$$

$R_{\square}$ is called sheet resistance.

Table 2.2: Resistivity and conductivity of some of the material.

Material	Resistivity (ρ) (Ω·m)	Conductivity (σ) (S/m)
Metals		
1. Silver	1.59×10^{-8}	$6.30 \times 10^{+7}$
2. Copper	1.68×10^{-8}	$5.96 \times 10^{+7}$
3. Gold	2.44×10^{-8}	$4.11 \times 10^{+7}$
4. Aluminium	2.65×10^{-8}	$3.77 \times 10^{+7}$
5. Tungsten	5.60×10^{-8}	$1.79 \times 10^{+7}$
Semiconductors		
1. P3HT	10^{+5}–10^{+6}	10^{-6}–10^{-5}
2. Gallium arsenide	10^{-3}–10^{+8}	10^{-8}–10^{+3}
3. Germanium	4.6×10^{-1}	2.17
4. Silicon	$2.3 \times 10^{+3}$	4.35×10^{-4}
5. Silicon carbide	10^{+2}–10^{+8}	10^{-8}–10^{-2}
Insulators		
1. Alumina	10^{+12}–10^{+15}	10^{-12}
2. Wood	10^{+14}–10^{+16}	10^{-16}–10^{-14}
3. Glass	10^{+11}–10^{+15}	10^{-15}–10^{-11}
4. Rubber	10^{+13}	10^{-14}
5. Teflon	10^{+23}–10^{+25}	10^{-25}–10^{-23}

2.6 Sheet Resistance, $R_{\square}$, of Thin Films

$R_{\square}$ is a crucial electrical characteristic that is used to describe conducting and semiconducting material sheets. $R_{\square}$ is a helpful parameter for comparing various thin films of material [58]. If $R_{\square}$ and thickness are known for a material, then its resistivity and conductivity can be calculated. Any thin film of material in which electrical charges are meant to move along the material (rather than flow through it) must possess $R_{\square}$. For instance, conducting electrodes are needed for thin film technologies (such as perovskite solar cells or OLEDs), and these electrodes typically have thicknesses in the nano–micrometre range. The electrodes must move

electrical charge laterally, and they require low $R_{\square}$ to minimise losses. When trying to scale up the size of these devices, this becomes even more crucial because the electrical charges will need to travel further along the electrodes before they can be extracted [59]. The chemical composition of thin films, the amount and kind of impurities present within or on their surface, the crystal structure of the thin film, and the kinds and densities of structural flaws are all factors that affect their electrical properties [60]. $R_{\square}$ is the material's resistivity given its geometrical dimensions.

Theoretical and practical interests have long existed in the electrical characteristics of thin films. The solid-state revolution has given thin film electrical conductors, insulators, and devices significant new functions. Microscopic thin film-based integrated circuit chips have replaced huge discrete electrical components and systems in a way that is more efficient and reliable. No matter the type of material, its physical state, or whether it is in bulk or film form, when a concentration of carriers n (number/m^3) with charge q moves past a specified reference plane with a velocity v (m/s) in response to an applied electric field E (V/m), it is said to flow an electric current of density J (A/m^2).

The straightforward relationship $J = nqv$ can be used to express the current flow's magnitude. The carrier velocity is proportional to E for the majority of materials, especially at low electric fields, meaning that $v = \mu E$. Here μ is the mobility, which is often referred to as the proportionality constant or velocity per unit field. As a result, $J = nq\mu E$ and by Ohm's law ($J = \sigma E$), the reciprocal of the resistivity ρ, or conductivity σ, is given by $\sigma = \frac{1}{\rho} = nq\mu$. The nature, size, and characteristics of the material constants in these equations are all sought to be defined by quantitative theories of electrical conductivity. The n, v or μ varies as a function of temperature,

composition, defect structure, and electric field. Comprehensive explanations of conduction integrate what may be called the "charge carrier dynamics" approach with the band structure viewpoint, and also incorporate electronic band structure considerations, which have successfully predicted property differences. The bulk conduction knowledge that has already been accumulated provides a solid foundation for understanding thin film behaviour. However, there are significant distinctions that give thin films distinctive qualities, and these are listed below:

1) Size effects or phenomena that develop because of the physically small dimensions at play. Examples include surface scattering and quantum mechanical tunnelling of charge carriers.

2) Film preparation method: The electrical characteristics of metal and insulator films depend on how they are deposited or formed, and this point cannot be emphasised enough. Different levels of crystal perfection, structural and electronic defect concentrations, dislocation densities, void or porosity content, density, grain morphology, chemical composition and stoichiometry, electron trap densities, eventual contact reactions, etc., result in materials with dramatically different properties, depending on the conditions used. Metals are less impacted by these effects than insulators, such as oxides and nitrides.

3) Electrode effects. In many cases, the substrate and a subsequent conducting film that is deposited act as electrodes for the questioned film that is sandwiched between them. Insulating films cannot generally be thought of independently from the electrodes that come into contact with them. The particular metal or semiconductor electrode materials used have a significant impact on the electrical response of devices including insulator or oxide layers between metals, semiconductors, and mixed electrodes. Some of the elements that can change the nature of charge

transport at an interface include interfacial adhesion, tension, interdiffusion, and integrated or adsorbed contaminants.

4) Discontinuous, island-structure films have different film continuity-conduction methods than continuous films.

5) The existence of high electric field conduction phenomena. High field effects are easily accessible in films due to the combination of moderate voltages applied over extremely small dimensions.

6) Due to corrosion, water vapour absorption, atmospheric oxidation and sulfidation, and low-temperature solid state processes, high chemical reactivity-films are vulnerable to ageing or time-dependent changes in electrical characteristics. Almost always, thin insulating films are more conductive than their corresponding bulk equivalents, and thin metal films are more resistant. Compared to insulators, metals have very few changes in film and bulk electrical characteristics. The electrical characteristics of thin films have been measured using a variety of approaches, some of which are modifications of popular techniques used with bulk materials.

For insulating films, electrodes are positioned on the opposing film surfaces of the films, where current travels through the film thickness. Small circular electrodes that have been evaporated or sputtered are typically used as a pair of equivalent contacts; the substrate usually serves as the other contact. A guard electrode is necessary if charge leaks from contact to contact along the surface, preventing through-film conduction. For more conductive metal and semiconductor films, all electrodes are often placed on the same film surface. These measurements use four terminals – two for current flow and two for voltage sensing. Reporting values of thin film resistivity in terms of $R_{\square}$ with the measurement is a fairly popular practice [35].

2.6.1 Measurement of Sheet Resistance, $R_{\square}$

$R_{\square}$ can be measured using contact methods such as the van der Pauw method, and the four-point probe method. There exist non-contact methods too - when the film that needs to be measured is either very thin, delicate, or buried beneath an insulating body, non-contact measurement techniques are particularly appealing.

Within a typical electrical system, the power supply takes on a certain function. It is the foundation of the system in many ways. By consistently and reliably powering the system's circuits, it gives the system life. Within a power supply system, the following three main power supply technologies can be taken into account:

1) Linear

Generally, linear regulators are utilised in ground-based equipment when low efficiency and heat generation are not big issues and where low cost, and a rapid design cycle are sought. In distributed power systems when the distributed voltage is less than 40 V direct current, they are quite common as board-level regulators. For the safety of producing dielectric isolation from the alternating current power line, a power supply stage ahead of the linear regulator must be provided for off-line (plug into the wall) devices. Each linear regulator can only produce one output voltage, and they can only produce output values that are lower than their input voltages. The typical efficiency of a linear regulator is between 35 % and 50 %. The loss is converted to heat energy.

2) Pulse Width Modulated (PWM) switching power supplies

Compared to linear regulators, PWM switching power supplies are far more flexible and efficient. They are frequently used in portable products, items for the aviation and automotive industries, compact instruments, offline applications, and practically any application that calls for great efficiency and multiple output voltages. Their

weight is substantially smaller than that of linear regulators since they require less heatsinking for the same output ratings. However, they do cost more to make and take longer to build from an engineering standpoint.

3) High-efficiency resonant technology switching power supplies

This variant of the standard PWM switching power supply finds use in applications that call for still-lightweight, smaller sizes and, most crucially, applications that call for a lower level of radiated noise (interference). These power supply units are frequently used in items like spacecraft electronics, portable, lightweight equipment, and avionics. The disadvantages of this power supply method include the fact that it often costs more than the other two technologies and necessitates the most technical design effort [61].

A constant current supply functions as a regulated current source. It is a power supply that puts out a constant flow (current) regardless of the pressure (voltage) [62]. A voltmeter's resistance should ideally be infinite to prevent it from affecting the circuit current. Only when measuring voltage in the case of a circuit with relatively extremely low resistance can a low resistance voltmeter provide an accurate measurement. When connected to a circuit whose resistance is similar to the resistance of the circuit, the voltmeter gives inaccurate and unreliable readings. This is due to the fact that the voltmeter will operate as a shunt path for the current when its resistance is less than or equal to the circuit's resistance, resulting in a voltage drop across the resistor where the measurement is required. The voltage drop will be less than the actual/true value as a result (value of resistance by theory or value of resistance before the voltmeter is connected). The loading effect is the name given to this phenomenon [63]. The above applies to the in-line four-point probe and square four-point probe setups. The current source must have a compliance voltage that is

significantly greater than may be anticipated for the four-point probe approach, and the input resistance of the voltmeter must be significantly larger. The issue arises if the sample's extremely high input resistance matches the electrometer voltmeter's input resistance in magnitude [64].

2.6.2 van der Pauw Method

In flat, arbitrary-shaped samples, the van der Pauw resistivity measurement technique is applied [36]. To apply this approach, the following four requirements must be met:

1) The sample needs to be flat and have a uniform thickness

2) The sample must be continuous, meaning there can be no isolated holes in it

3) The sample must be homogeneous and isotropic

4) The sample's edges must host each of the four connections.

Along with these other four requirements, any one contact's area of contact must be at least an order of magnitude lower than the area of the entire sample. This might not be practical or possible for small samples. It is still possible to do precise van der Pauw resistivity measurements even if the contacts cannot be made any smaller by employing geometric correction factors to take into account the contacts' finite size. Attaching four contacts to the four corners of a sheet of material in the shape of a square is a more typical geometry. To perform a van der Pauw measurement, the following steps are followed:

1) Define a resistance $R_{ij,kl...}$ V_{kl}/I_{ij}, where $V_{kl...}$ $V_k–V_l$ is the voltage between points k and l, and I_{ij} is the current flowing from contact i to contact j

2) Measure the resistances $R_{21,34}$ and $R_{32,41}$. Define $R_>$ as the greater of these two resistances and $R_<$ as the lesser of these two resistances

3) Calculate the ratio $R_>/R_<$ and find the corresponding value of the function $f(R_>/R_<)$

4) Calculate the resistivity ρ_a using:

$$\rho_a = \frac{\pi d(R_> + R_<) f(R_>/R_<)}{\ln 4} \tag{2.16}$$

where ρ_a = Resistivity in $\Omega \cdot m$

d = Thickness of the sample in meters

Resistances $R_>$ and $R_<$ are measured in Ω

$\ln 4 \cong 1.3\,863$.

It is not necessary to measure the width or length of the sample.

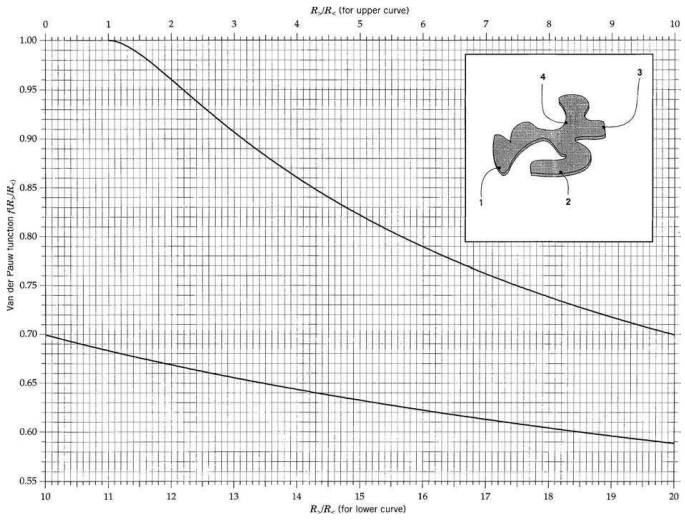

Figure 2-14: The graph shows the function $f(R_>/R_<)$ needed to solve for the resistivity in equation (2.17) [58].

5) To measure $R_{43,12}$ and $R_{14,23}$, switch the leads. To calculate ρ_b using these updated values for $R_>$ and $R_<$, repeat steps 3 and 4. The sample is either too irregular for a reliable measurement or either the contacts are bad if the two resistivities, ρ_a and ρ_b, are not within 10 % of one another. Make new contacts. If the two resistivities ρ_a and ρ_b are within 10 % of each other, the best estimate of the material resistivity ρ is the average:

$$\rho = \frac{(\rho_a + \rho_b)}{2} \tag{2.17}$$

$$f(R_>/R_<) \equiv \frac{-\ln 4(R_>/R_<)}{\left[1+(R_>/R_<)\ln\left\{1-4^{-[(1+R_>/R_<)f]^{-1}}\right\}\right]} \tag{2.18}$$

2.6.3 Four-Point Probe Method

Wenner [65] first employed the four-point probe method in 1916 to measure the earth's resistivity. It was utilised by Valdes [66] for the measurement of semiconductor wafer resistivity in 1954. The semiconductor industry uses it frequently today to keep an eye on the manufacturing process [67]. The four-point probe technique can be used to test thin film thickness, although it is commonly employed to measure the $R_\square$ of shallow layers (as a result of epitaxy, ion-implant, diffusion, evaporation or sputtering) and the bulk resistivity of bare wafers [36]. Eliminating contact/wire resistance is one of the four-point probe method's main benefits.

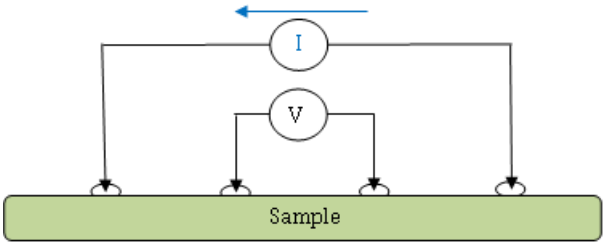

Figure 2-15: The in-line four-point probe instrument is depicted schematically [37].

A typical in-line four-point probe instrument is shown in figure 2-15 above and contains four co-linear, equally spaced probes that make electrical contact with the substance to be characterised. As mentioned previously a high impedance voltmeter is used to measure the voltage across the two inner probes caused by the application of a DC constant current through the outer probes, which allows $R_{\square}$ to be calculated.

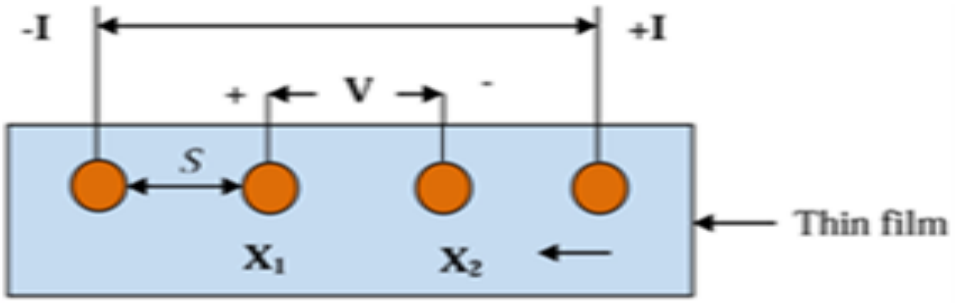

Figure 2-16: A schematic of a four-point probe design with linear symmetry [36].

Considering figure 2-16 above, the metal tip is considered to be infinitesimal for bulk samples, and samples are semi-infinite in the lateral dimension. It is anticipated that the current will protrude spherically from the outer probe tips when the sample thickness, $t >> S$, and the probe spacing match. After that, the differential resistance is provided by:

$$\Delta R = \rho_{\square} \left(\frac{dx}{A}\right) \tag{2.19}$$

where, $\rho_{\square}$ is the sheet resistivity, A is the area of the film and dx is the separation between X_1 and X_2. Integration between the inner probes used to measure the voltage yields the following results:

$$R_{\square} = \int_{x_1}^{x_2} \rho \frac{dx}{2\pi x^2} \tag{2.20}$$

$$R_{\square} = \frac{\rho}{2\pi}\left(-\frac{1}{x}\right)\Big|_{x_1}^{x_2} \tag{2.21}$$

$$R_{\square} = \frac{\rho}{2\pi}\left(-\frac{1}{x}\right)\Big|_{S}^{2S} \tag{2.22}$$

$$R_{\square} = \frac{\rho}{2\pi}\frac{1}{2S} \tag{2.23}$$

$$R = \frac{V}{2I} \tag{2.24}$$

where S stands for the uniform probe spacing. Due to the superposition of current at the outer two tips, $R = \frac{V}{2I}$ Thus, we arrive at the following definition for bulk resistivity:

$$\rho_{\square} = 2\pi S\left(\frac{V}{I}\right) \tag{2.25}$$

Figure 2-17 illustrates four probes on a square shaped sample for the determination of sheet resistance.

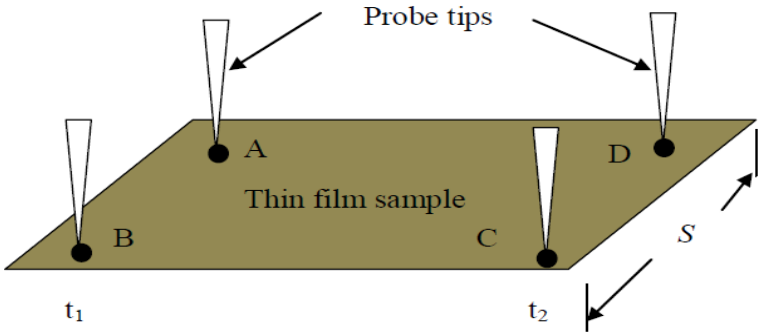

Figure 2-17: Probe tips on the square-shaped film sample surface [36].

We have current rings rather than spheres when we consider a thin film with square geometry, as in figure 2-17, with a very thin layer (thickness, t << probe spacing, S). hence, the area,

$$A = 2\pi xt \tag{2.26}$$

$$R_{\square} = \int_{x_1}^{x_2} \rho \frac{dx}{2\pi xt} \tag{2.27}$$

$$= \int_{S}^{2S} \frac{\rho}{2\pi t} \frac{dx}{x} \tag{2.28}$$

$$= \frac{\rho}{2\pi t} \ln(x)\Big|_{S}^{2S} \tag{2.29}$$

$$= \frac{\rho}{2\pi t} \ln 2 \tag{2.30}$$

As a result, for $R = \frac{V}{2I}$ The thin film sheet resistivity is determined by:

$$\rho_{\square} = \frac{\pi t}{\ln 2}\left(\frac{V}{I}\right) \tag{2.31}$$

It should be noted that the probe spacing S has no effect on this expression. Sheet resistivity is typically represented as:

$$\rho_{\square} = K\left(\frac{V}{I}\right) \tag{2.32}$$

where K is a geometrical factor. K = 4.532, or simply $\frac{\pi}{\ln 2}$ follows from the derivation in the case of a semi-infinite thin sheet. In the case of imperfect samples, the factor K will change. As a result, equations (2.33) and (2.34) can be used to express the $R_{\square}$ and $\rho_{\square}$, respectively.

$$R_{\square} = 4.532\left(\frac{V}{I}\right) \tag{2.33}$$

$$\rho_{\square} = 4.532t\left(\frac{V}{I}\right) \tag{2.34}$$

Despite the fact that equation (2.33) for $R_{\square}$ is independent of sample geometry, this only holds true if the sample is much thinner than 40 % of the probe spacing and if its dimensions are 40 times greater than the probe spacing. If not, the proximity to

the sample's edges limits the potential current routes between the probes, which causes an overestimation of the $R_{\square}$. A correction factor based on the sample's geometry is needed to adjust for this discrepancy. Since there is no equation for a rectangular sample, calculating the geometrical correction factor is a little more challenging. An empirically derived table of correction factors can be used as an alternative. For example: The probe spacing is $s = 2$ mm, and the rectangular sample has a long edge of $l = 20$ mm and a short edge of $w = 10$ mm. Since $l/w = 2$ and $w/s = 5$ in this instance, the empirical table (table C1) is searched for the correction factor that fulfils these two values, finding $K = 0.7887$ along the columns for $l/w = 2$ and the rows for $w/s = 5$. To obtain the accurate value for the sample, the measured $R_{\square}$ is multiplied by this number. Not all samples will neatly fit into one of these categories. In this situation, it is advised to determine the proper correction factor for the sample using cubic spline interpolation. It's crucial to keep in mind that the correction factors for rectangular samples in table C1 only apply to readings made in the sample's centre. Different correction factors are required if the measurement is not centred [68].

2.7 Sheet Resistance, $R_{\square}$ and the Thickness of Thin Films

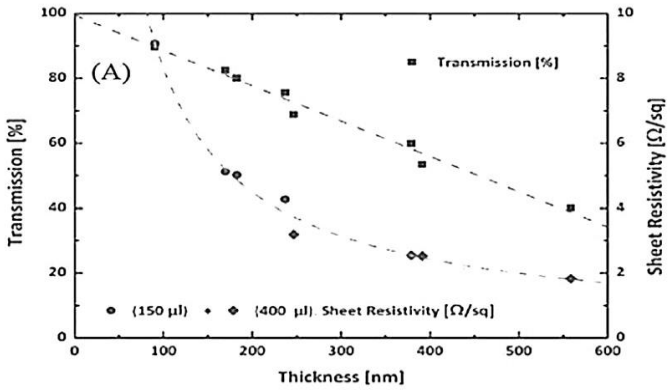

Figure 2-18: Influence of layer thickness on $R_{\square}$ and optical transmission of silver nanowires [69].

Figure 2-18 depicts that the $R_{\square}$ reduces as a power of thickness, which is attributed to the increase in the number of silver-nanowire connections, which increases the conductivity [69].

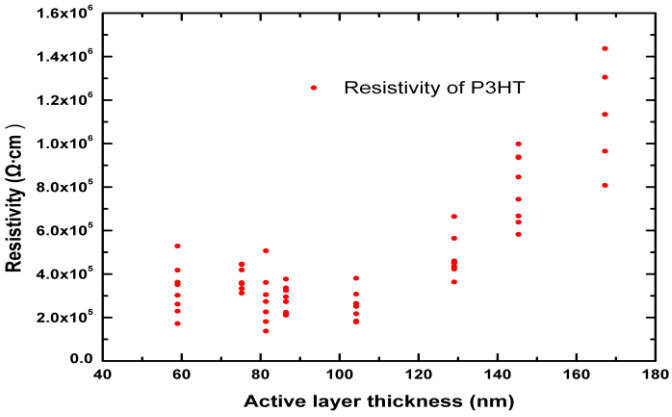

Figure 2-19: P3HT device (ITO/P3HT/Al) resistivity with various P3HT layer thicknesses [70].

The 1.20×10^{-7} m cross point is easier to detect in figure 2-19. The resistivity of P3HT can be estimated by deducting the contact resistance and accounting for the

thickness of the P3HT layer. The resistivity of P3HT does not change when the active layer is thinner than 1.20×10^{-7} m, which is expected as resistivity for most crystals should not change with material thickness. In the case of conjugate polymers, this rule does not, however, hold true. The resistivity increases quickly for active layers with a thickness greater than 1.20×10^{-7} m cases. That is, the dominant recombination is the cause of the resistivity's quick growth [70]. Electrical conductivity is tested in samples made from P3HT polymer and is a function of the thickness of the P3HT layers, demonstrating that the conductivity of P3HT polymer thin films rises with thickness [71].

2.8 Chapter Summary

This chapter delved extensively into the study's literature review. Since their 1970s discovery, conductive polymers have undergone much research. Researchers have been particularly interested in P3HT because of the favourable prospective features that make it suitable for use in OPVs. Compared to their bulk counterparts, thin films offer unique features. Physical vapour deposition, chemical vapour deposition, oxidation, wet processing, and plating are a few of the techniques used to create thin films. The P3HT thin films' characteristics are influenced by the solvent used to create the P3HT solution. The majority of the time, optical techniques are used to measure the thickness of thin films $R_{\square}$ in thin films is a beneficial characteristic. The van der Pauw and four-point probe methods are typically used to calculate $R_{\square}$. For the majority of materials, there is a power relationship between $R_{\square}$ and thin film thickness.

CHAPTER 3 : RESEARCH METHODS

This chapter explains the methodology used for the study. The research design, methods, data analysis, and research ethics are all shown in depth.

3.1 Research Design

The quantitative research design was used. The commercial P3HT was dissolved in $CHCl_3$. P3HT thin films of various thicknesses were fabricated by the spin coating method on glass substrates. For each thin film, its thickness was determined, and $R_{\square}$ was measured, and the tabulated data collected were analysed with descriptive and inferential statistics, and then conclusions were reached.

3.2 Procedure

3.2.1 Dissolving of P3HT

1.2×10^{-5} Kg of P3HT (MW = 60.15, 97.6 % RR) purchased from Ossila Ltd was put into a vial. 1.0×10^{-3} L of $CHCl_3$ solvent obtained from LABTECH was added to the vial. Hence a P3HT solution with concentration of 1.2×10^{-2} Kg/L was made. The closed vial was put on the Benchmark magnetic stirrer with a stirrer bar and heated at 343.15 K for 1 800 s inside the fume hood, afterwards, the vial was left on the magnetic stirrer with a stirrer bar overnight at 303.15 K inside the dark fume hood to prevent excessive aggregation of the P3HT molecules.

3.2.2 Fabrication of P3HT Thin Films

Eight glass slides with the square dimensions of 2.5×10^{-2} m by 2.5×10^{-2} m were cut into size by using the Matus glass cutter and marked with numerals in order from 1 to 8 with the Würth tungsten scriber and were sonicated in the Scientech ultrasonic bath with a detergent at 353.15 K for 300 s, and then rinsed in hot deionized water, and then in cold deionized water. The glass slides were then sonicated again in acetone for 300 s at 329.15 K and then rinsed in deionized water twice, they were again sonicated in 2-Propanol for 300 s at 343.15 K and then rinsed in deionized water twice, and then placed in deionized water to be stored until they were needed, when needed, they were blown dry with a nitrogen gas gun. Eight thin film samples with 1.2×10^{-2} Kg/L concentration of 1.0×10^{-4} L P3HT solution each were spin coated on the square 2.5×10^{-2} m by 2.5×10^{-2} m glass slides as substrates in a Kyowa Riken K-35951 spin coater, using the parameters in table 3.1 below.

Table 3.1: Spin coating parameters for the prepared P3HT thin film samples.

Glass sample #	First spin coating step for 10 s at spin coater rotational speed ω (rpm)	Second spin coating step for 30 s at spin coater rotational speed ω (rpm)
1	500	2 000
2	750	2 000
3	1 000	2 000
4	1 250	2 000
5	1 500	2 000
6	1 750	2 000
7	2 000	2 000
8	2 250	2 000

Estimated P3HT thin film samples of thicknesses were between 6.0×10^{-8} m–1.2×10^{-7} m.

3.2.3 Determination of the Thickness of P3HT Thin Films

Each glass slide was weighed on the Mettler Toledo AT201 max = 205 g, d = 0.01 mg electronic balance to obtain its weight before and after the spin coating procedure. The P3HT thin film samples were annealed in the oven at 423.15 K for 600 s. The annealed P3HT thin film samples were weighed on the Mettler Toledo AT201 max = 205 g, d = 0.01 mg electronic balance to obtain their weights. The thicknesses of the as-cast and annealed P3HT thin film samples were calculated by using equation (2.11) from the mass changes of the substrate (before and after the spin coating, and annealing procedures) and the P3HT thin film samples' thicknesses were also estimated by using equation (2.10), called the spin coating equation for thickness from the ω obtained from the spin coater.

3.2.4 Measurement of Sheet Resistance, $R_{\square}$ of P3HT Thin Films

A dual in-line four-point probe head was designed and fabricated. The four-point probe head has an in-line 2.0×10^{-3} m of equidistant spacing between the probes, the probes have 0.1 Kg of spring force and are 7.39×10^{-4} m in diameter.

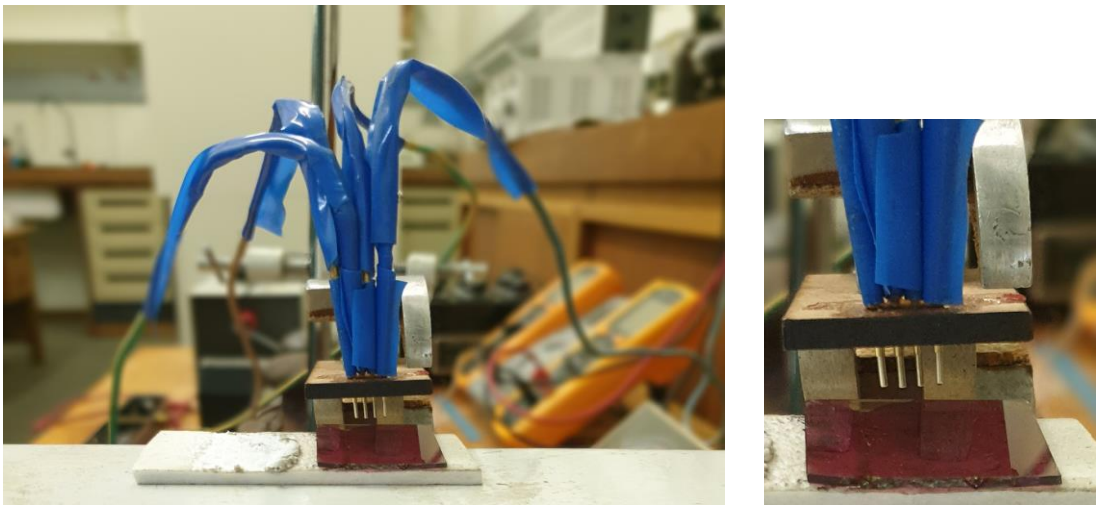

Figure 3-1: The picture of the fabricated in-line four-point probe head.

The $R_{\square}$ of all the eight P3HT thin film samples was measured using the designed and fabricated four-point probe head with the ISOTECH and Leybold current sources and Toptronic multimeters (MMs). The $R_{\square}$ measurements were done in 132 lx of light from the fluorescent bulbs with indirect sunlight, and inside the dark room, for both as-cast and annealed P3HT thin film samples. The geometric factor was added to the measurements (from table C1). The measurements were done at 1 µA, 2 µA, 3 µA, and 4 µA constant currents for each of the eight P3HT thin film samples.

3.3 Data Analysis

Quantitative data analysis was used. The mean for each data set was calculated for accuracy and precision. Standard deviation was applied to the data for error analysis. Regression was used to get the dependence between the thickness and $R_{\square}$ on each other. Regression was used when plotting the graphs.

3.4 Research Ethics

Ethical clearance was obtained from the UNAM Research Ethics Committee, and research Permission from the Postgraduate Support Services. All waste generated in the laboratory was disposed of according to the guidelines for waste disposal of the Standard Operation Procedure document number SOP-29-1 and UNAM Occupational Safety and Health guidelines. All experiments were conducted in a well-ventilated and sterilised fume hood, and safety protective clothing was used.

3.5 Chapter Summary

The chapter showed that the quantitative research design was used. The P3HT solution was prepared. Fabrication of P3HT thin film samples was made by spin coating. Varying the coating ω varies the thicknesses of P3HT thin film samples, the in-line four-point probe head was designed and fabricated, then used to measure $R_{\square}$. Regression, means, standard deviation and curve fitting were used. Research ethics were followed, and a research permission letter was obtained.

CHAPTER 4 : RESULTS AND DISCUSSIONS

This chapter presents the results obtained from the study and explains how the data was analysed. The findings from the results are covered in this chapter. The chapter also highlights the restrictions and goes into explaining how outcomes compare to the literature.

Tables 4.1–4.4 show the calculated $R_{\square}$ for the P3HT thin films from the measured readings (tables D1–D4) using equation (2.33). The $R_{\square}$ is calculated at 1 µA, 2 µA, 3 µA, and 4 µA constant currents. Tables 4.1–4.4 also show the P3HT thin films sample number, the estimated P3HT thin films' thicknesses, and the P3HT thin films' coating ω.

Table 4.1: Calculated $R_{\square}$ for the as-cast P3HT thin films for the measurements done in the light.

P3HT Thin Film			$R_{\square}$ (10^{+6}) (Ω/□)			
Thin film sample #	Thickness (nm)	Spin coater rotational speed ω (rpm)	At 1 µA	At 2 µA	At 3 µA	At 4 µA
1	120	500	0.395	0.856	1.05	1.04
2	100	750	0.527	0.980	1.30	1.47
3	90	1 000	2.37	2.24	2.27	2.59
4	80	1 250	3.03	2.24	2.97	3.53
5	72	1 500	4.21	3.93	4.20	4.71
6	70	1 750	3.86	3.29	4.15	5.18
7	62	2 000	5.27	3.36	3.66	3.85
8	60	2 250	3.34	2.41	2.91	2.60

Table 4.2: Calculated $R_{\square}$ for the as-cast P3HT thin films for the measurements done in the dark.

P3HT Thin Film			$R_{\square}$ (10^{+6}) ($\Omega/\square$)			
Thin film sample #	Thickness (nm)	Spin coater rotational speed ω (rpm)	At 1 µA	At 2 µA	At 3 µA	At 4 µA
1	120	500	0.965	0.900	1.13	1.10
2	100	750	2.46	1.93	1.42	1.48
3	90	1 000	2.72	1.82	2.03	2.50
4	80	1 250	4.21	3.53	3.06	3.24
5	72	1 500	3.60	3.84	4.18	4.49
6	70	1 750	4.48	3.09	4.40	4.25
7	62	2 000	4.65	3.84	3.26	3.47
8	60	2 250	4.21	3.12	2.55	2.18

Table 4.3: Calculated $R_{\square}$ for the annealed P3HT thin films for the measurements done in the light.

P3HT Thin Film			$R_{\square}$ (10^{+6}) ($\Omega/\square$)			
Thin film sample #	Thickness (nm)	Spin coater rotational speed ω (rpm)	At 1 µA	At 2 µA	At 3 µA	At 4 µA
1	120	500	0.176	0.351	0.366	0.428
2	100	750	0.439	0.461	0.512	0.538
3	90	1 000	0.263	0.417	0.614	0.790
4	80	1 250	0.395	0.790	0.746	1.25
5	72	1 500	0.614	1.29	1.76	2.17
6	70	1 750	1.05	1.27	2.18	2.44
7	62	2 000	1.97	2.39	2.91	2.58
8	60	2 250	1.71	1.97	2.28	2.62

Table 4.4: Calculated $R_{\square}$ for the annealed P3HT thin films for the measurements done in the dark.

P3HT Thin Film			$R_{\square}$ (10^{+6}) ($\Omega/\square$)			
Thin film sample #	Thickness (nm)	Spin coater rotational speed ω (rpm)	At 1 µA	At 2 µA	At 3 µA	At 4 µA
1	120	500	1.23	1.05	0.951	1.03
2	100	750	1.40	1.54	1.80	2.13
3	90	1 000	1.80	1.97	2.22	2.22
4	80	1 250	3.03	2.68	2.91	2.80
5	72	1 500	2.94	2.33	2.85	2.95
6	70	1 750	3.07	2.24	2.97	3.03
7.	62	2 000	2.55	2.85	2.62	3.21
8.	60	2 250	2.59	1.93	1.83	1.99

Tables 4.1–4.4 show that the $R_{\square}$ is calculated at four various constant currents, which means the measurements were done at 1 µA, 2 µA, 3 µA, and 4 µA constant currents instead of only one constant current. This is done to reduce errors in that various constant currents further enhance the clarity of the phenomenon being investigated. The smaller the constant current used to obtain $R_{\square}$ the more accurate $R_{\square}$ becomes, so the four constant currents chosen are within the relevant limits. In general, the thickness of a spin coated film is proportional to the inverse of the square root of ω, as in equation (2.10).

According to Griffin et al. [47] if and when the fabrication of a thin film is done with great precautions then the equation (2.10) could be used to obtain the thin film thickness. Figure 2-11 shows a graph of ω versus thin film thickness that was obtained by Griffin et al. using equation (2.10). Hence the thin film thickness could be obtained from their ωs. Two different thin films (with the same ω = 750 rpm) with

similar fabrication conditions' $R_{\square}$ were calculated from the measured readings obtained and the values fluctuates but not so much at all. Another two different thin films (with the same ω = 2 000 rpm) with similar fabrication conditions' $R_{\square}$ were calculated from the measured readings obtained and the values fluctuates but not so much at all.

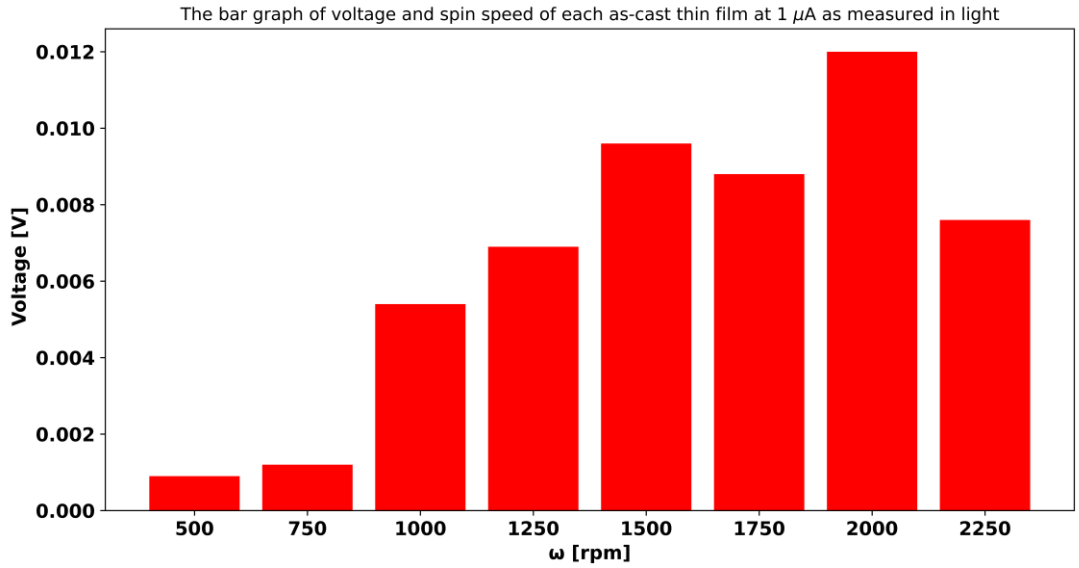

Figure 4-1: The bar chart of voltage and ω at 1 μA for as-cast P3HT thin films for the measurements done in the light.

It is clearly shown in figure 4-1 above that as the ω increases (whereby the thicknesses of the P3HT thin films are reduced), the voltages tend to increase most of the time, the measurements were done in the light for as-cast P3HT thin films, as determined at 1 μA. This implies that indeed the current became limited when the thicknesses of the P3HT thin films were reduced. The resistivity of the P3HT thin films does not have a strong dependence on the thicknesses of the P3HT thin films, the electrical conductivity is given by $\sigma = \mu nq$, where μ is the mobility, n is the

concentration of charge carriers and q is the charge. Since the conductivity is the inverse of the resistivity, i.e., $\rho = \frac{1}{\sigma}$ it too has a weak dependence on the P3HT thin films' thicknesses. The $R_{\square}$ has a strong dependence on both the P3HT thin films' thicknesses and the resistivity so it has a strong dependence on the conductivity as well. As the thicknesses of the P3HT thin films increased it was seen that the insulative behaviour of the P3HT thin films subsides a little, and the P3HT thin films' conductivity increased, $R_{\square}$ tended to become smaller.

Figure 4-2 below shows that as the ω increases the $R_{\square}$ tends to increase too, the measurements were done in the light for as-cast P3HT thin films, and it shows the $R_{\square}$ as determined at four different constant currents.

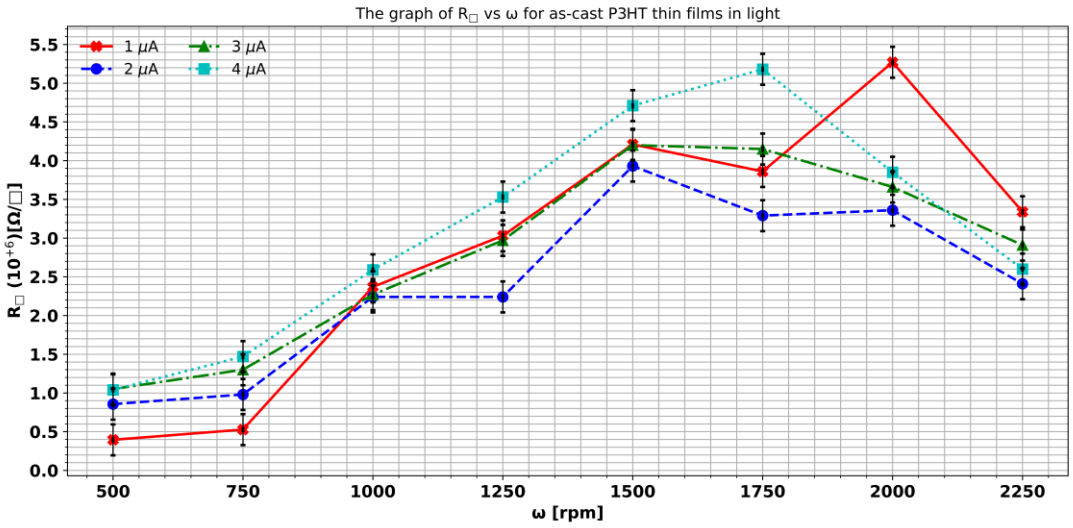

Figure 4-2: The graph of $R_{\square}$ vs ω for as-cast P3HT thin films for the measurements done in the light.

Figure 4-3 below shows that as the ω increases the $R_{\square}$ tends to increase too, the measurements were done in the dark for as-cast P3HT thin films, and it shows the $R_{\square}$ as determined at four different constant currents.

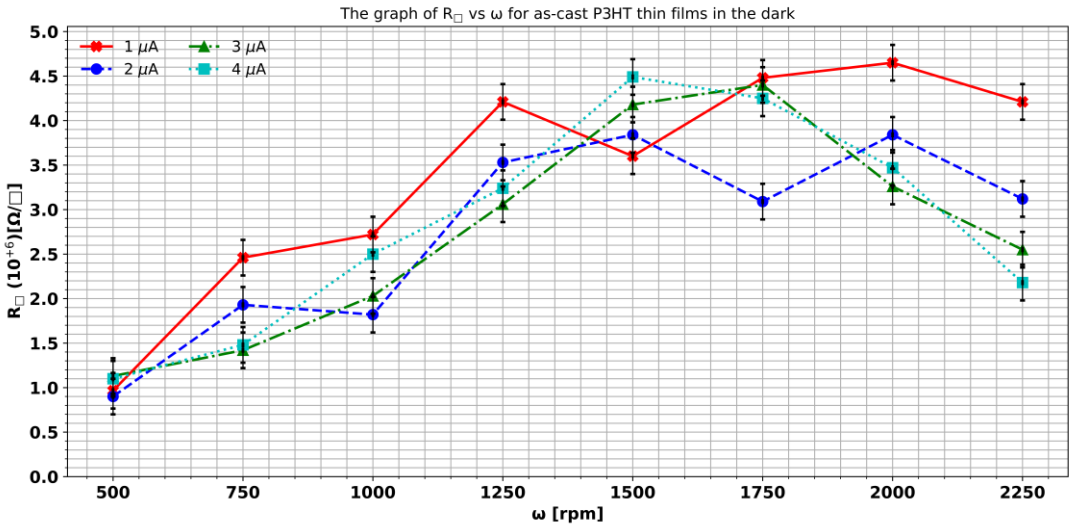

Figure 4-3: The graph of $R_{\square}$ vs ω for as-cast P3HT thin films for the measurements done in the dark.

Figure 4-4 below shows that as the ω increases the $R_{\square}$ tends to increase too, the measurements were done in the light for annealed P3HT thin films, and it shows the $R_{\square}$ as determined at four different constant currents.

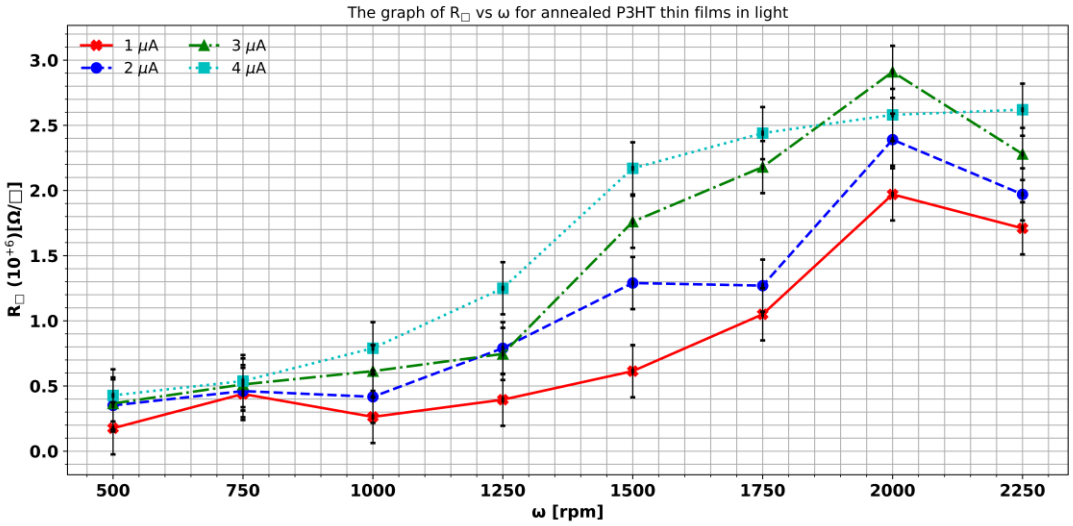

Figure 4-4: The graph of $R_{□}$ vs ω for annealed P3HT thin films for the measurements done in the light.

Figure 4-5 below shows that as the ω increases the $R_{□}$ tends to increase too, the measurements were done in the dark for annealed P3HT thin films, and it shows the $R_{□}$ as determined at four different constant currents.

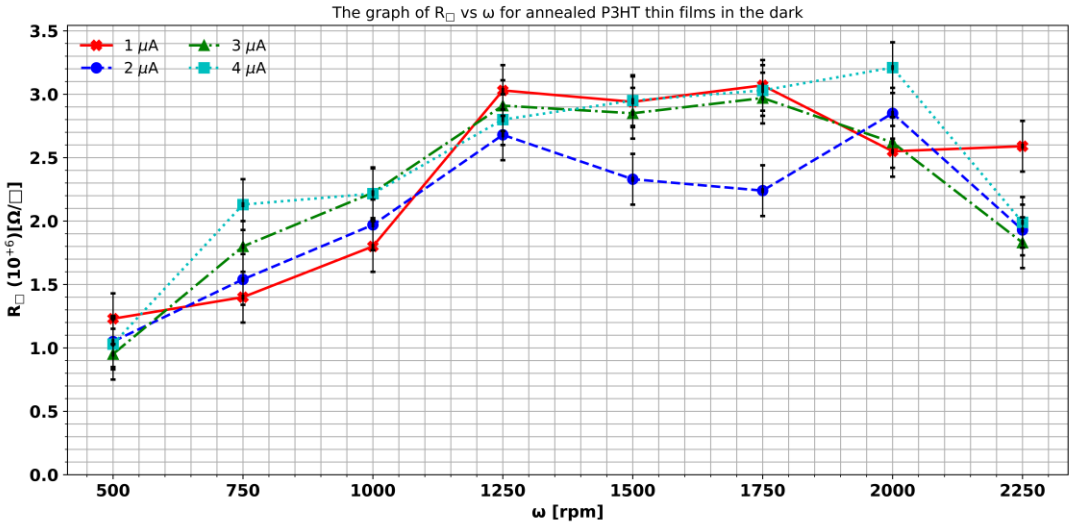

Figure 4-5: The graph of $R_{□}$ vs ω for annealed P3HT thin films for the measurements done in the dark.

Since the P3HT thin films' thicknesses reduce as the ω increases, then the inverse of the ω depicts the increasing order of the P3HT thin films' thicknesses, figure 4-6 below shows that the $R_{\square}$ of the P3HT thin films tends to decrease as the P3HT thin films' thicknesses increase, the measurements were done in the light for as-cast P3HT thin films, it shows the $R_{\square}$ as determined at four different constant currents.

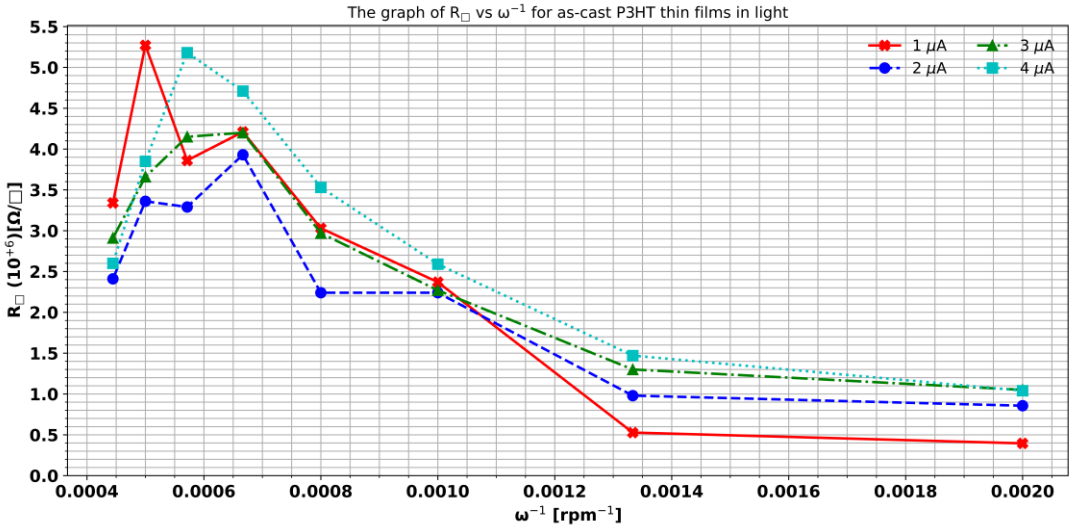

Figure 4-6: The graph of $R_{\square}$ vs ω^{-1} for as-cast P3HT thin films for the measurements done in the light.

Figure 4-7 below shows that the $R_{\square}$ of the P3HT thin films tends to decrease as the P3HT thin films' thicknesses increase, the measurements were done in the dark for as-cast P3HT thin films, and it shows the $R_{\square}$ as determined at four different constant currents.

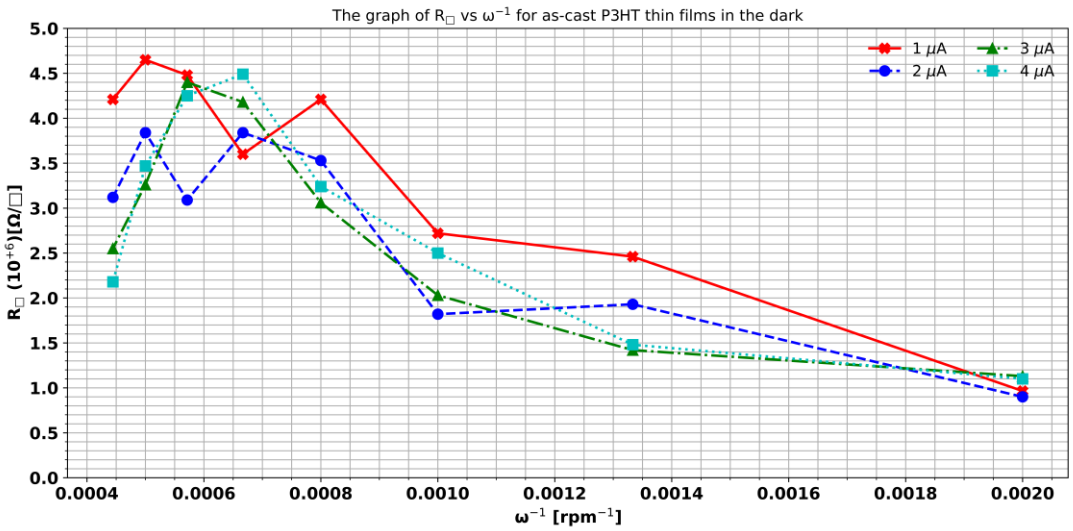

Figure 4-7: The graph of $R_{\square}$ vs ω^{-1} for as-cast P3HT thin films for the measurements done in the dark.

Figure 4-8 below shows that the $R_{\square}$ of the P3HT thin films tends to decrease as the P3HT thin films' thicknesses increase, the measurements were done in the light for annealed P3HT thin films, and it shows the $R_{\square}$ as determined at four different constant currents.

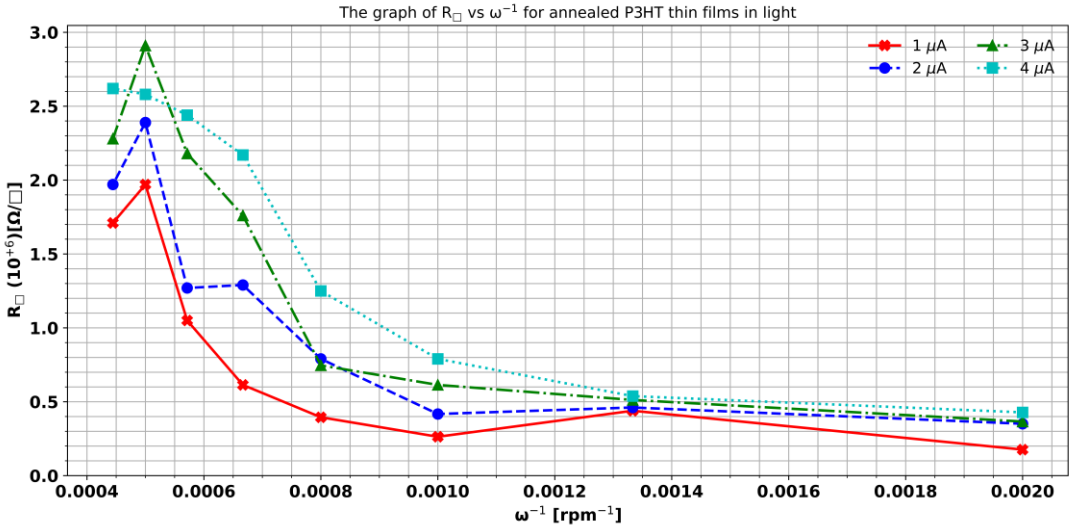

Figure 4-8: The graph of $R_{\square}$ vs ω^{-1} for annealed P3HT thin films for the measurements done in the light.

Figure 4-9 below shows that the $R_{\square}$ of the P3HT thin films decreases as the P3HT thin films' thicknesses increase, the measurements were done in the dark for annealed P3HT thin films, and it shows the $R_{\square}$ as determined at four different constant currents.

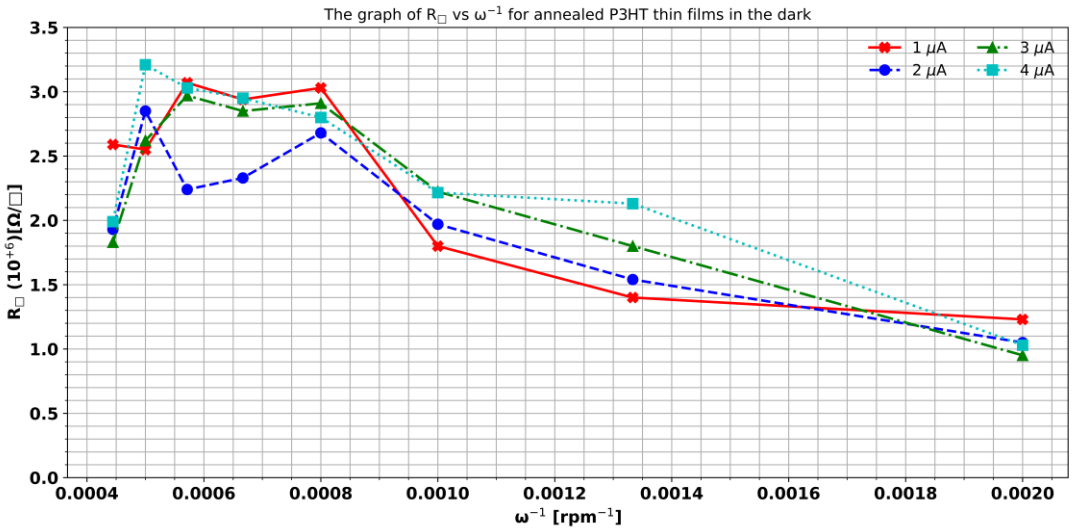

Figure 4-9: The graph of $R_{\square}$ vs ω^{-1} for annealed P3HT thin films for the measurements done in the dark.

In figures 4-2 to 4-9, it is shown that the $R_{\square}$ decreased as the P3HT thin films' thicknesses increased, this can be attributed to that the more material available or given the more charge carriers are available or given [35]. P3HT produces photo generated charge carriers since it absorbs in radiation within the visible wavelength range, and this may influence the current of the P3HT thin films, so measuring the $R_{\square}$ in the dark and light reveals this phenomenon. In P3HT applications, knowing the different values of $R_{\square}$ in light and dark is useful. The measurement of $R_{\square}$ in the dark seems to lose a little dependence on the P3HT thin films' thicknesses, and this could

be because the P3HT is less conductive in the dark since the creation of positive charge carriers (p-type) of P3HT seizes [20][72], which throws the four-point probe method measurements off balance which develops with little outlier points as well, the four-point probe method does not measure $R_{\square}$ well for insulative material [58], the overall $R_{\square}$ increases in the dark. P3HT thin films show a weaker connection between $R_{\square}$ and the thicknesses of the thin films, unlike thin metallic films which show a strong connection between $R_{\square}$ and thin films' thicknesses [69][70].

Figures 4-10 to 4-17 illustrate the curve fitting for $R_{\square}$ vs ω and $R_{\square}$ vs ω^{-1} graphs for as-cast and annealed P3HT thin films for the measurements performed in the light and the dark.

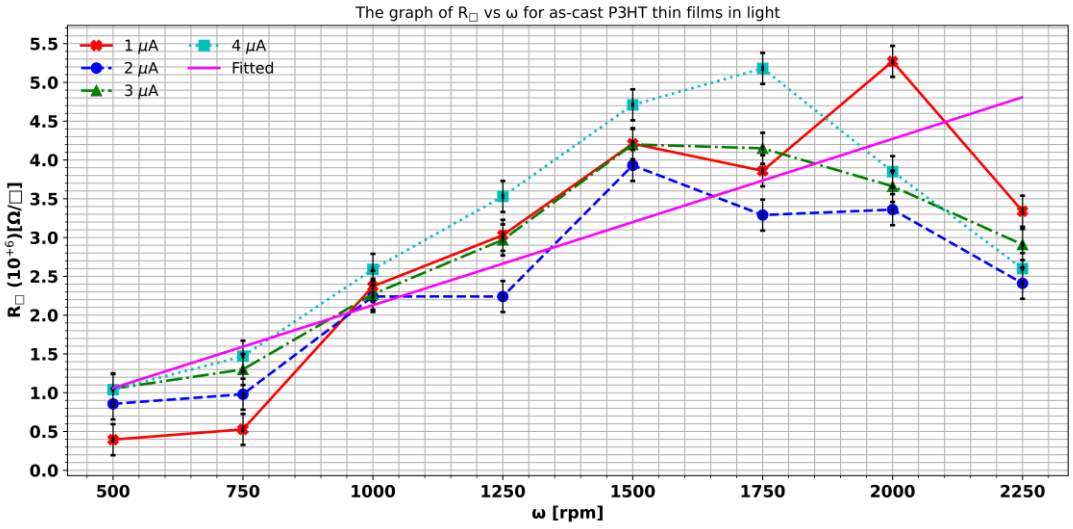

Figure 4-10: The graph of $R_{\square}$ vs ω for as-cast P3HT thin films for the measurements done in the light with curve fitting.

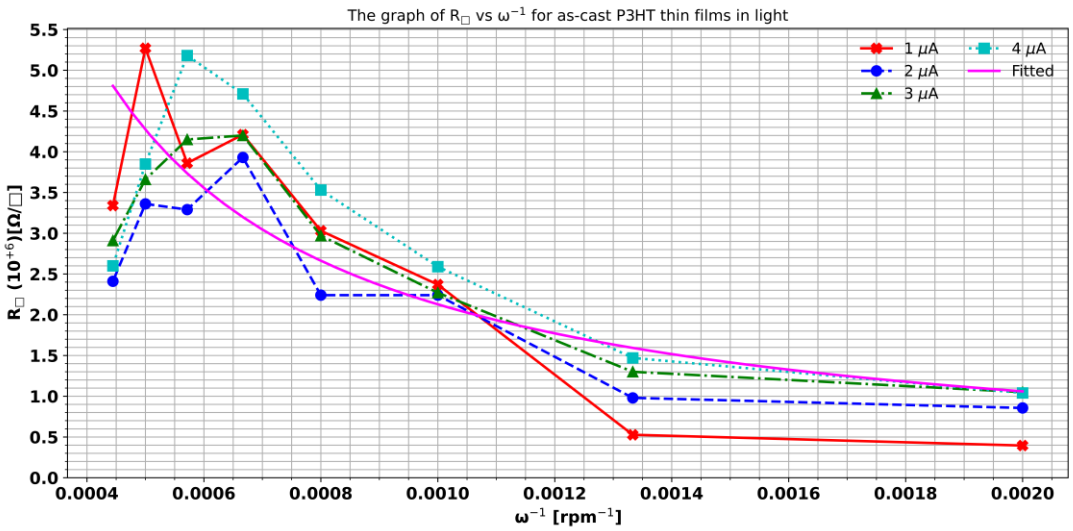

Figure 4-11: The graph of $R_{\square}$ vs ω^{-1} for as-cast P3HT thin films for the measurements done in the light with curve fitting.

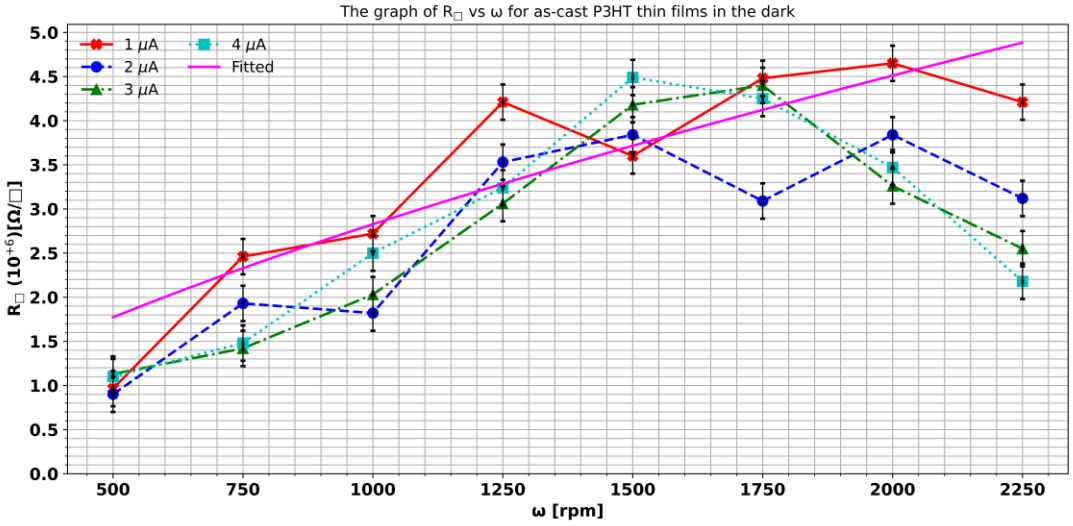

Figure 4-12: The graph of $R_{\square}$ vs ω for as-cast P3HT thin films for the measurements done in the dark with curve fitting.

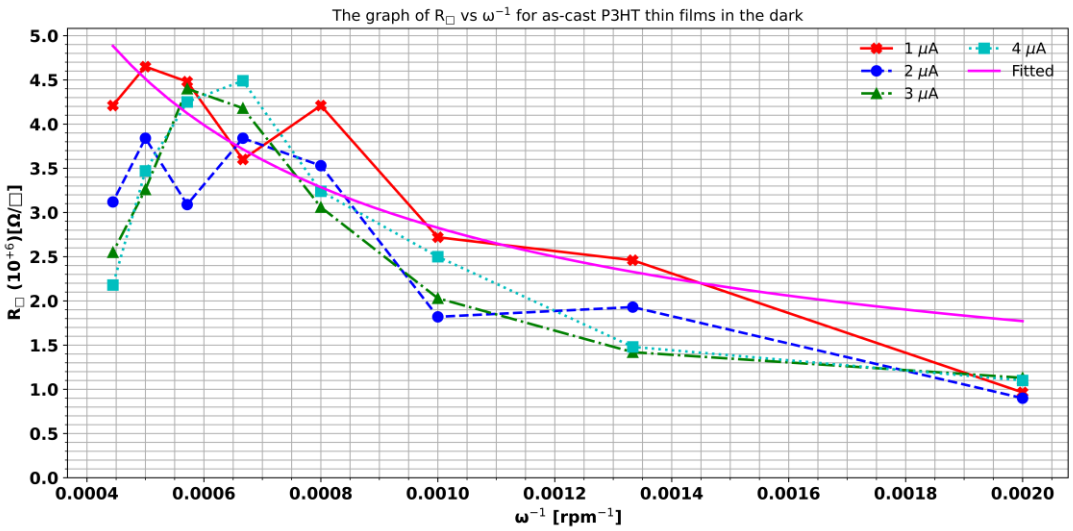

Figure 4-13: The graph of $R_{\square}$ vs ω^{-1} for as-cast P3HT thin films for the measurements done in the dark with curve fitting.

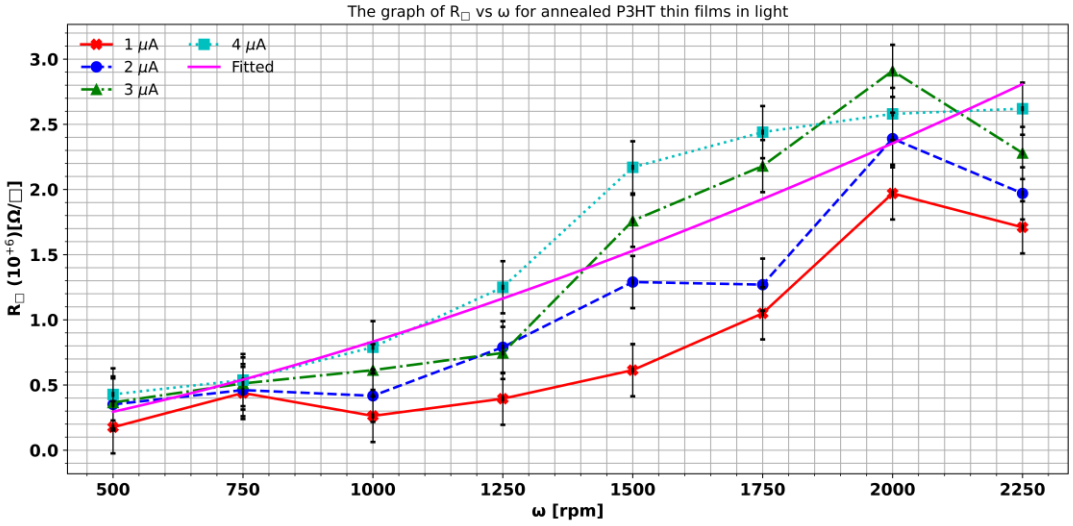

Figure 4-14: The graph of $R_{\square}$ vs ω for annealed P3HT thin films for the measurements done in the light with curve fitting.

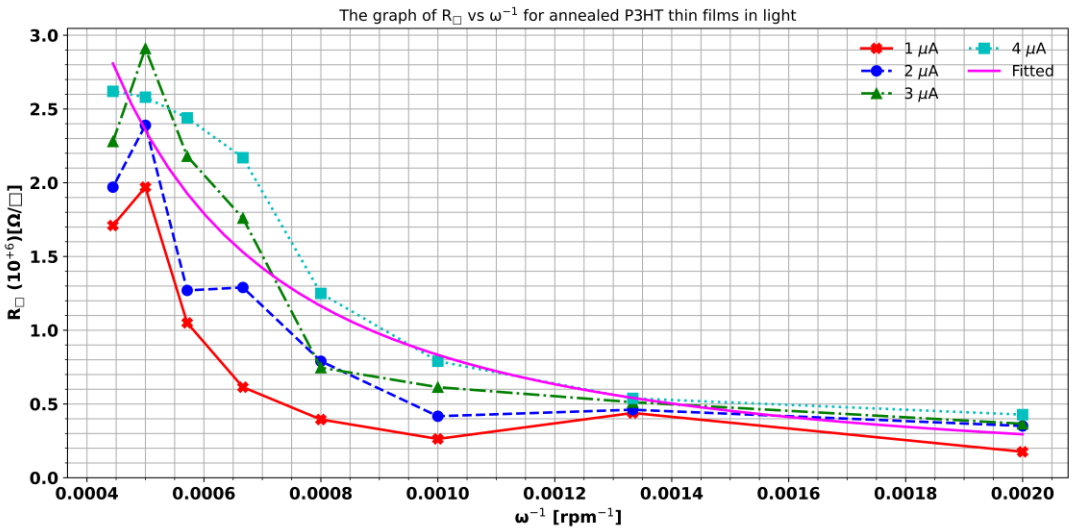

Figure 4-15: The graph of $R_{\square}$ vs ω^{-1} for annealed P3HT thin films for the measurements done in the light with curve fitting.

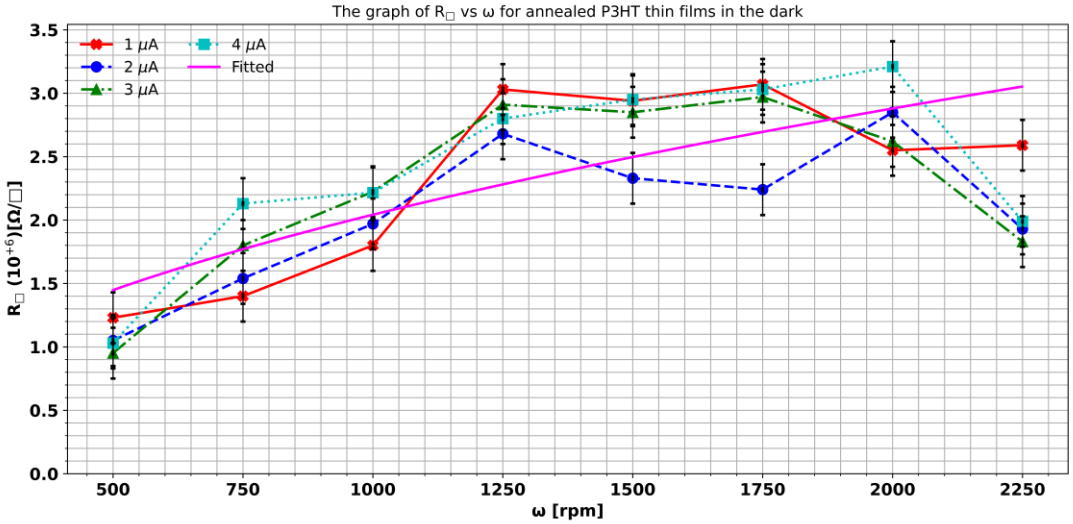

Figure 4-16: The graph of $R_{\square}$ vs ω for annealed P3HT thin films for the measurements done in the dark with curve fitting.

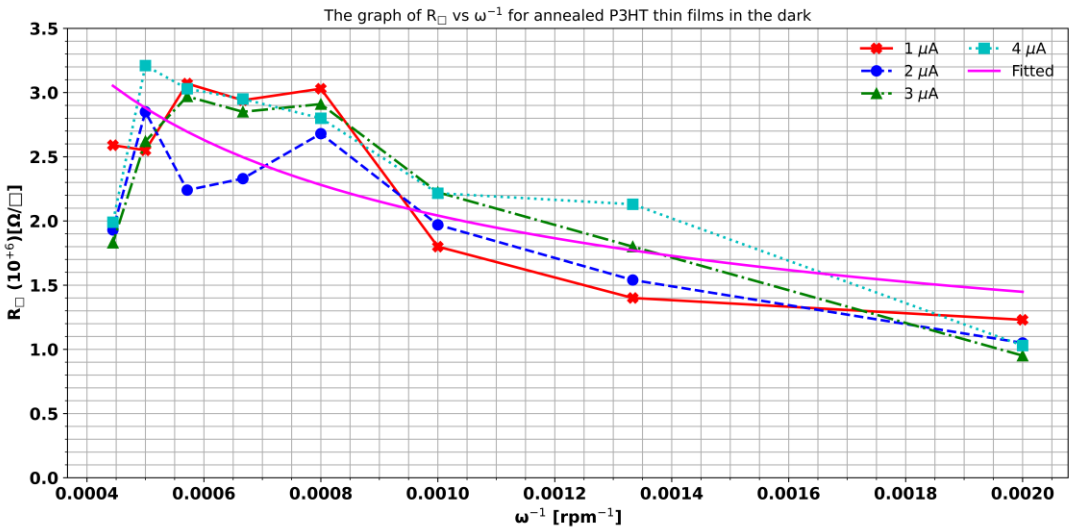

Figure 4-17: The graph of $R_{\square}$ vs ω^{-1} for annealed P3HT thin films for the measurements done in the dark with curve fitting.

In figures 4-10 to 4-17, the curve fitting was done in the Python programming language. Curve fitting allows the observation and quantification of the behaviour of the physical phenomena of the situation. Curve fitting eliminates the noise from the dataset. Curve fitting fixes measured data to an analytical equation to extract meaningful parameters. The compatibility of the graphs with the curve fitting models demonstrates the existence of a pattern between $R_{\square}$ and the P3HT thin films' thicknesses. The correlation between the $R_{\square}$ and the P3HT thin films' thicknesses is much clearer when the P3HT thin films are annealed because the conductivity of the P3HT thin films increases [25], and the four-point probe method becomes more accurate and precise. The $R_{\square}$ decreases after the annealing of P3HT thin films. Initial annealing of the P3HT thin films increases the $R_{\square}$, the heat evaporates away the remaining solvent from the P3HT thin films, and the water vapour and the oxygen are also removed from the P3HT thin films, but all of these impurities contribute to the decrease of the $R_{\square}$ because they contribute to the increment of the conductivity of

the P3HT thin films due to them introducing more charge carriers. Further heating recrystallises the P3HT [31], making the threads more likely to be in contact with each other and any contact on the P3HT thin films increases the conductivity of the P3HT thin films and decreases the resistivity and the $R_{\square}$.

The P3HT dissolved in $CHCl_3$ as a solvent is a Newtonian fluid [47], which influences the wet spin coating of the P3HT thin films. The spin coating method produces uniform thin films, uniform P3HT thin films produce more precise and accurate findings when measuring the $R_{\square}$ of P3HT thin films. $CHCl_3$ is the best solvent for P3HT since it dissolves it better than the other solvents, this allows the P3HT to crystalise better hence allowing for improved conductivity of P3HT [41]. The solvent utilised for dissolving the P3HT polymer and the fabrication method both impact the measured $R_{\square}$ [41]. The resistivity of the P3HT thin films depends on the rate of deposition, temperature, thickness, and grain [73].

The $R_{\square}$ makes it easier to get resistance for materials with known square dimensions. The optimal $R_{\square}$ makes it easier to transfer and collect charges from material for solar cells, since it is the surface resistance [74]. The low charge mobility of conductive organic polymers limits the active-layer thickness of the solar cells and light absorption [64]. The P3HT is almost insulative so the measurement results depend on the accuracy of the measurement devices i.e., MM, the material of the probes, contact with the sample, the voltage applied, surface contamination and electrostatic charging and interfacial tension. The errors of the experiment are that the whole fabrication and measurement were not done in a nitrogen gas environment, even though all care was implemented to prevent damage to the thin films, the probes could crack the thin films, and the wiring of the setup also could introduce errors, due to the non-availability of standard equipment that could estimate the thicknesses

of the P3HT thin films. The $R_{\square}$ for the annealed P3HT thin films and as-cast P3HT thin films were measured and obtained, and the P3HT thin films' thicknesses were estimated by the mass of P3HT coated on the substrates using equation (2.11) and from the spin coating thickness equation (2.10). Spin coating is better for thin film coating, but it wastes a lot of material on a large-scale, doctor blading could replace it on a larger fabricating scale [47].

4.1 Chapter Summary

In this chapter, the results from the performed experiments used were shown. The analysis of the results was also illustrated. It was shown that $R_{\square}$ correlates with the P3HT thin films' thicknesses. The outlier points only occur between those points with a small ω gap difference. The relationship between the thin film thicknesses and the $R_{\square}$ is a power curve for all the set conditions. The $R_{\square}$ decreases as the thin film thickness increases. $R_{\square}$ decreases for post-treated (annealed) P3HT thin films. $R_{\square}$ is bigger for the measurements done in the dark than in the light.

CHAPTER 5 : CONCLUSIONS AND RECOMMENDATIONS

The conclusions gathered from doing the study are stated in this chapter. The future recommendations from the study are also discussed.

The work aimed to fabricate P3HT thin films of different thicknesses, measure the $R_{\square}$ of each P3HT thin film, and determine the thicknesses of each P3HT thin film. This was satisfied by the methods as follows: Eight P3HT thin films with various thicknesses were fabricated by the spin coating method and varying the speed, ω, of the spin coater for each P3HT thin film ensured that their thicknesses were also varied. The P3HT thin films were annealed in an oven. The four-point probe setup was designed, fabricated, and then used to measure the $R_{\square}$ for the eight P3HT thin films of different thicknesses. The holder for the P3HT thin films in the four-point probe setup had cushioned surface and a screw knob that allowed it to move up and down ever so slightly, this allowed the four-point probe head not to damage the thin films. In turn, the four probes had a rounded tip and spring load to prevent any more damage to the P3HT thin films. The whole setup was connected to a power supply and MMs.

The $R_{\square}$ for the P3HT thin films measured ranged from $3.95 \times 10^{+5}$ Ω/□ to $5.27 \times 10^{+6}$ Ω/□ for the as-cast P3HT thin films and from $1.76 \times 10^{+5}$ Ω/□ to $3.21 \times 10^{+6}$ Ω/□ for the annealed P3HT thin films. The P3HT thin films' thicknesses ranged between 6.0×10^{-8} m–1.2×10^{-7} m approximately. The $R_{\square}$ decreased as the P3HT thin films' thicknesses increased. The measured $R_{\square}$ decreased after annealing the P3HT thin films. The $R_{\square}$ increased a little when measured in the dark for P3HT thin films. The bulk resistance of P3HT dissolved in $CHCl_3$ as measured with the MM was $1.47 \times 10^{+9}$ Ω using the four-point probe method circuit under light illumination. The correlations "r" for the graphs are high enough, ranging from 0.90–0.99, which was

calculated using Microsoft Excel software. Knowing how the $R_{\square}$ behaves in the dark, and in the light, and with the change in thicknesses of P3HT thin films material, allows its engineered applications outside the research laboratory. The $R_{\square}$ is a very much useful tool in electrical engineering and other fields. Knowing the $R_{\square}$ of material reduces measurements required in a particular electrical manipulation, it can easily be measured, with no need to know the size of the sample or its thickness.

The four-point probe method can be used to characterise the unknown materials when the thickness is known. However, more results could be obtained if more sophisticated measuring equipment and isolated conditions in the laboratory could be used. The room for improvement is highlighted below with the following suggestions for future work:

- The effect of optical absorption on the generation of charge carriers for a large range of voltages/threshold fields.
- Analysis of the effect of sheet resistance under varying ranges of temperature (100–300 K) and in the presence of light illumination or the dark.
- Effect of structural conformation using vibrational spectroscopy and also electron transport methods such as photoluminescence
- Role of co-solvent on morphology modification in P3HT and the $R_{\square}$.

References

[1] BP 2019 BP Statistical Review of World Energy Online: https://www.bp.com/content/dam/bp/business sites/en/global/corporate/pdfs/energy-economics/statistical-review/bp-stats-review-2019-global-insights accessed on 02 October 2020

[2] National Center for Photovoltaics 2004 What is the Energy Payback for PV ? Online: http://www.nrel.gov/docs/fy05osti/37322 accessed on 25 October 2020

[3] Kaushik B K, Kumar B, Negi Y S and Mittal P 2012 Prospects and Limitations of Organic Thin Film Transistors (OTFTs) *Adv. Comput. Sci.* **167** 125–39

[4] Smith R, Inomata H and Peters C 2013 *Introduction to Supercritical Fluids* vol 4, ed R Smith, H Inomata and C Peters (Elsevier Science)

[5] Sims L, Egelhaaf H J, Hauch J A, Kogler F R and Steim R 2012 Plastic Solar Cells ed A Sayigh *Compr. Renew. Energy* **1** 439–80

[6] IUPAC Recommendation 1980 1981 IUPAC Stereochemical Definitions and Notations Relating to Polymers *Pure Appl. Chem.* **53** 733–52

[7] Dodeja K, Bishnoi P and Bhola Y 2020 *Polymer Chemistry* (Beau Bassin: LAP LAMBERT Academic Publishing)

[8] Brinkmann M 2011 Structure and Morphology Control in Thin Films of Regioregular Poly(3-hexylthiophene) *J. Polym. Sci. Part B Polym. Phys.* **49** 1218–33

[9] Gnanou Y and Fontanille M 2008 *Organic and Physical Chemistry of*

Polymers (Hoboken: John Wiley & Sons, Inc)

[10] Mark J J, Allcock H R and West R 2005 *Inorganic Polymers* (New York: Oxford University Press)

[11] Pethrick R A 2010 *Polymer Science and Technology for Scientists and Engineers* (Dunbeath: Whittles Publishing)

[12] Monika, Kumar R, Chauhan R P, Kumar R and Chakarvarti S K 2010 Synthesis of Conducting Polymers and Their Characterization *Indian J. Pure Appl. Phys.* **48** 524–6

[13] Margolis J 1989 *Conductive Polymer and Plastics* ed J Margolis (London: Chapman and Hall)

[14] Awuzie C I 2017 Conducting Polymers *Mater. Today Proc.* **4** 5721–6

[15] Márquez O and Márquez J 2007 Properties of Organic Conducting Polymers *Adv. Eng. Sci.* **1** 1–14

[16] Wan M 2008 *Conducting Polymers With Micro or Nanometer Structure* (Berlin: Springer Berlin, Heidelberg)

[17] McCullough R D 1998 The Chemistry of Conducting Polythiophenes *Adv. Mater.* **10** 93–116

[18] Pankow R M and Thompson B C 2020 The Development of Conjugated Polymers as the Cornerstone of Organic Electronics *Polymer (Guildf).* **207** 122874

[19] Guo X, Baumgarten M and Müllen K 2013 Designing π-Conjugated Polymers for Organic Electronics *Prog. Polym. Sci.* **38** 1832–908

[20] Ahmed M F 2013 *Evaluation of Transport Properties in Poly(3-*

hexylthiophene) Using SCLC Method and Controlled-Overflow-Transistor Licentiate Thesis (Universidade Federal do Paraná)

[21] Okutan M, Yerli Y, San S E, Yilmaz F, Günaydin O and Durak M 2007 Dielectric Properties of Thiophene Based Conducting Polymers *Synth. Met.* **157** 368–73

[22] Kumar M, Velaga S and Singh A 2022 A Study of Thickness Dependent Microstructure of Poly(3-hexylthiophene) Thin Films Using Grazing Incidence X-ray Diffraction *Soft Mater.* **20** 24–34

[23] Davoise L V, Capilla R P and Díez-Pascual A M 2021 Assessment of Optical Properties of Graphene-Poly(3-hexylthiophene) Nanocomposite Applied to Organic Solar Cells *Mater. Proc.* **3** 3–6

[24] Österholm J E, Passiniemi P, Isotalo H and Stubb H 1987 Synthesis and Properties of $FeCl_4$-Doped Polythiophene *Synth. Met.* **18** 213–8

[25] Aruna P and Joseph C M 2017 Annealing Effects on the Electrical Properties of Spin Coated Poly(3-hexylthiophene) (P3HT) Thin Films *Mater. Sci. Semicond. Process.* **61** 39–44

[26] Fonsêca de C M J and Alves dos P A da S M 2018 Influence of Solvent Used on Oxidative Polymerization of Poly(3-hexylthiophene) in Their Chemical Properties *Polimeros* **28** 395–9

[27] Ansari M A, Mohiuddin S, Kandemirli F and Malik M I 2018 Synthesis and Characterization of Poly(3-hexylthiophene): Improvement of Regioregularity and Energy Band Gap *RSC Adv.* **8** 8319–28

[28] Jang K S, Eom Y S, Lee T W, Kim D O, Oh Y S, Jung H C and Nam J Do 2009 Fabrication of Poly(3-hexylthiophene) Thin Films by Vapor-Phase

Polymerization for Optoelectronic Device Applications *ACS Appl. Mater. Interfaces* **1** 1567–71

[29] Chiguvare Z, Parisi J and Dyakonov V 2003 Current Limiting Mechanisms in Indium-Tin-Oxide/Poly3-hexylthiophene/Aluminum Thin Film Devices *J. Appl. Phys.* **94** 2440–8

[30] Motaung D E, Malgas G F and Arendse C J 2011 Insights Into the Stability and Thermal Degradation of P3HT:C60 Blended Films for Solar Cell Applications *J. Mater. Sci.* **46** 4942

[31] Chiguvare Z, Parisi J and Dyakonov V 2007 Influence of Thermal Annealing on the Electrical Properties of Poly(3-hexylthiophene)-Based Thin Film Diodes *Zeitschrift fur Naturforsch.* **62** 609–19

[32] Joshi S, Grigorian S and Pietsch U 2008 X-ray Structural and Crystallinity Studies of Low and High Molecular Weight Poly(3-hexylthiophene) *Phys. Status Solidi Appl. Mater. Sci.* **205** 488–96

[33] Tarek A and Mabdoua Y 2020 *The Analytical Study of the Laser Flash Method* (Algiers)

[34] Moshfegh A Z, von Känel H, Kashyap S C and Wuttig M 2003 Physics and Technology of Thin Films *Proceedings of the International Workshop on Physics and Technology of Thin Films* ed A Z Moshfegh, H von Kanel, S C Kashyap and M Wuttig (Tehran: World Scientific Publishing Co.)

[35] Ohring M 1992 *The Materials Science of Thin Films* (San Diego: Academic Press)

[36] Agumba J O 2010 *Design and Fabrication of a Simple Four Point Probe System for Electrical Characterization of Thin Films* MSc. Thesis (Kenyatta

University)

[37] Naftaly M, Das S, Gallop J, Pan K, Alkhalil F, Kariyapperuma D, Constant S, Ramsdale C and Hao L 2021 Sheet Resistance Measurements of Conductive Thin Films : A Comparison of Techniques *Electronics* **10** Online: http://dx.doi.org/10.3390/electronics10080

[38] Teixeira C O, Castro D, Andrade L and Mendes A 2022 Selection of the Ultimate Perovskite Solar Cell Materials and Fabrication Processes Towards its Industrialization: A Review *Energy Sci. Eng.* **10** 1478–525

[39] Roncaselli L K M, Silva E A, Ramanitra H H, Stephen M, Simõis A V S, Bégué D D, Agostini D L S, Hiorns R C and Olivati C A 2021 Study of the Effect of Solvent on the Conductivity of Langmuir-Schaefer Films of Poly(Fullerene)s *Mater. Res.* **24** 1–6

[40] Jiemsakul T, Jiramitmongkon K, Asawapirom U and Chotsuwan C 2017 Investigation of P3HT Electrochromic Polymer Films Prepared by Ultrasonication of Polymer Solutions *J. Mater. Sci.* **52** 8485–92

[41] Jang M, Huh Y-I and Chang M 2020 Effects of Solvent Vapor Annealing on Morphology and Charge Transport of Poly(3-hexylthiophene)(P3HT) Films Incorporated With Preformed P3HT Nanowires *Polymers (Basel).* **10** 1188

[42] Abdellah A, Fabel B, Lugli P and Scarpa G 2010 Spray Deposition of Organic Semiconducting Thin-Films: Towards the Fabrication of Arbitrary Shaped Organic Electronic Devices *Org. Electron.* **11** 1031–8

[43] Chan C K, Richter L J, Dinardo B, Jaye C, Conrad B R, Ro H W, David S G, Daniel A F, Dean M D and Gundlach D J 2010 High Performance Airbrushed Organic Thin Film Transistors *Appl. Phys. Lett.* **96** 133304

[44] Bielecka U, Lutsyk P, Janus K, Sworakowski J and Bartkowiak W 2011 Effect of Solution Aging on Morphology and Electrical Characteristics of Regioregular P3HT FETs Fabricated by Spin Coating and Spray Coating *Org. Electron.* **12** 1768–76

[45] Mitzi D B, Kosbar L L, Murray C E, Copel M and Afzali A 2004 High-Mobility Ultrathin Semiconducting Films Prepared by Spin Coating *Nature* **428** 299–303

[46] Hellstrom S L 2007 Basic Models of Spin Coating Online: http://large.stanford.edu/courses/2007/ph210/hellstrom1/ accessed on 10 November 2021

[47] Griffin J, Hassan H and Spooner E 2021 Spin Coating: Complete Guide to Theory and Techniques Online: https://www.ossila.com/pages/spin-coating#choosing-a-spin-coating-method accessed on 12 June 2022

[48] Emslie A G, Bonner F T and Peck L G 1958 Flow of a Viscous Liquid on a Rotating Disk *J. Appl. Phys.* **29** 858–62

[49] Meyerhofer D 1978 Characteristics of Resist Films Produced by Spinning *J. Appl. Phys.* **49** 3993–7

[50] Birnie D P and Manuel Manley 1997 Combined Flow and Evaporation of Fluid on a Spinning Disk *Phys. Fluids* **9** 870–5

[51] Horowitz F, Yeatman E, Dawnay E and Fardad A 1993 Real-Time optical monitoring of Spin coating *J. Phys.* **3** 2059–63

[52] Birnie D P 2001 Rational Solvent Selection Strategies to Combat Striation Formation During Spin Coating of Thin Films *J. Mater. Res.* **16** 1145–54

[53] Piegari A and Masetti E 1985 Thin Film Thickness Measurement: A Comparison of Various Techniques *Thin Solid Films* **124** 249–57

[54] AlSalhi M S, Aljaafreh M J and Prasad S 2020 Narrowband Spontaneous Emission Amplification From a Conjugated Oligomer Thin Film *Polymers (Basel).* **12** 232

[55] Flack W W, Soong D S, Bell A T and Hess D W 1984 A Mathematical Model For Spin Coating of Polymer Resists *J. Appl. Phys.* **56** 1199–206

[56] Hall D B, Underhill P and Torkelson J M 1998 Spin Coating of Thin and Ultrathin Polymer Films *Polym. Eng. Sci.* **38** 2039–45

[57] Scott R P 2012 *Measuring the Thickness of Thin Metal Films* BSc. Thesis (Brigham Young University)

[58] Heaney M B 2004 Electrical Conductivity and Resistivity *Electrical Measurement, Signal Processing, and Displays* ed Webster John G (Florida: CRC Press LLC) pp 7.1-7.14

[59] Ossila 2023 Calculate Sheet Resistance Using the Four-Probe Method Online: https://www.ossila.com/pages/sheet-resistance theory?_pos=1&_sid=c487bb0be&_ss=r#example-applications accessed on 29 March 2021

[60] Ogwu A A, Darma T H and Bouquerel E 2007 Electrical Resistivity of Copper Oxide Thin Films Prepared by Reactive Magnetron Sputtering *J. Achiev. Mater. Manuf. Eng.* **24** 172–7

[61] Brown M 2001 *Power Supply Cookbook* (Elsevier Inc)

[62] Calex 2001 Constant Current Power Supplies Online: https://calex.com/

accessed on 22 June 2022

[63] Dr. B. R. Ambedkar National Institute of Technology *Laboratory Manual for Voltmeter Resistance* (Jalandhar)

[64] Keithley 2017 High Resistance Measurements 1–8

[65] Wenner F 1915 A Method of the Measurement Earth Resistivity *Bull. Bur. Stand.* **12** 469–4

[66] Valdes L B 1954 Resistivity Measurements on Germanium for Transistors *Proc. IRE* **42** 420–7

[67] Smits F M 1958 Measurement of Sheet Resistivity With the Four Point Probes *Bell Syst. Tech. J.* 711–8

[68] Topsoe H 1966 Geometric Factors in Four Point Resistivity Measurement Online: https://www.iiserkol.ac.in/~ph324/StudyMaterials/GeometricFactors4ProbeResistivity.PDF accessed on 17 May 2022

[69] Basarir F, Irani F S, Kosemen A, Camic B T, Oytun F, Tunaboylu B, Shin H J, Nam K Y and Choi H 2017 Recent Progresses on Solution-Processed Silver Nanowire Based Transparent Conducting Electrodes for Organic Solar Cells *Mater. Today Chem.* **3** 60–72

[70] Yang S 2013 *Investigation of Electrical Properties of P3HT:PCPBM Organic Solar Cells* PhD Thesis (University of Virginia)

[71] Asane J, Peters V N, Rohan A, Wallace T N, Peters D and Noginov M A 2018 Study of Conductivity of the Poly(3-hexylthiophene-2, 5-diyl) Polymer (P3HT) in Resonant Fabry-Perot Cavities *SPIE Nanoscience + Engineering* p

107

[72] Ballantyne A M, Wilson J S, Nelson J, Bradley D D C, Durrant J R, Heeney M, Duffy W and McCulloch I 2006 TOF Mobility Measurements in Pristine Films of P3HT: Control of Hole Injection and Influence of Film Thickness *Org. Photovoltaics VII* **6334** 633408

[73] Grigorian S, Joshi S and Pietsch U 2010 Temperature-Dependent Structural Properties of P3HT Films *IOP Conf. Ser. Mater. Sci. Eng.* **14** 012007

[74] Gadisa A 2006 *Studies of Charge Transport and Energy Level in Solar Cells Based on Polymer/Fullerene Bulk Heterojunction* PhD Thesis (Linköping University)

Appendices

Appendix A

UNAM
UNIVERSITY OF NAMIBIA

ETHICAL CLEARANCE CERTIFICATE

Ethical Clearance Reference Number: SOS-0014 Date: 25 October 2021

This Ethical Clearance Certificate is issued by the University of Namibia Ethics Committee (REC) in accordance with the University of Namibia's Research Ethics Policy and Guidelines. Ethical approval is given in respect of undertakings contained in the Research Project outlined below. This Certificate is issued on the recommendations of the ethical evaluation done by the ethics committee.

Title of Project: INVESTIGATION OF THE DEPENDENCE OF SHEET RESISTANCE ON THE THICKNESS OF DOCTOR BLADED POLY(3-HEXYLTHIOPHENE) THIN FILMS

Student: OLIVER SIBENGA, MUTENDA

Student Number: 200118153

Supervisor(s): DR ZIVAYI CHIGUVARE (UNIVERSITY OF NAMIBIA)

Centre for Research Services
Take note of the following:

1. Any significant changes in the conditions or undertakings outlined in the approved Proposal must be communicated to the ethics committee. An application to make amendments may be necessary.
2. Any breaches of ethical undertakings or practices that have an impact on ethical conduct of the research must be reported to the ethics committee
3. The Principal Researcher must report issues of ethical compliance to the ethics committee (through the Chairperson) at the end of the Project or as may be requested by the ethics committee
4. The ethics committee retains the right to:

i) Withdraw or amend this Ethical Clearance if any unethical practices (as outlined in the Research Ethics Policy) have been detected or suspected,

ii) Request for an ethical compliance report at any point during the course of the research.

The ethics committee wishes you the best in your research.

Dr. Zivayi Chiguvare (Chairperson Ethics Committee)

Prof. Davis Mumbengegwi (Head, Multidisciplinary Research)

Appendix B

CENTRE FOR RESEARCH SERVICES
Office of the Pro-Vice Chancellor: Research, Innovation & Development
University of Namibia, Private Bag 13301, Windhoek, Namibia
340 Mandume Ndemufayo Avenue, Pioneers Park, Office F223 - Fblock, Second Floor
☎ +264 61 206 4673; E-mail:kmbulu@unam.na; URL.: http//www.unam.edu.na

UNAM
UNIVERSITY OF NAMIBIA

RESEARCH PERMISSION LETTER

Date: 11/04/2022

Student Name: OLIVER SIBENGA MUTENDA

Student Number: 200118153

Programme: MASTER OF SCIENCE IN PHYSICS

Approved Research Title: Investigation of The Dependence of Sheet Resistance on The Thickness of Doctor Bladed Poly(3-Hexylthiophene) Thin Films

TO WHOM IT MAY CONCERN

I hereby confirm that the above-mentioned student is registered at the University of Namibia for the programme indicated. The proposed study met all the requirements as stipulated in the University guidelines and has been approved by the relevant committees.

The proposal adheres to ethical principles as per attached Ethical Clearance Certificate. Permission is hereby granted to carry out the research as described in the approved proposal.

Best Regards

Dr. AEE Shikongo
Head: Postgraduate Support Services
Tel: +264 61 206 3129
E-mail: aeshikongo@unam.na

CENTRE FOR RESEARCH SERVICES
Office of the Director
2022 -04- 11
University of Namibia
UNAM

Appendix C

Table C1: Table of empirically determined correction factors [67].

w / s	l / w = 1	l / w = 2	l / w = 3	l / w = 4
1			0.2204	0.2205
1.25			0.2751	0.2751
1.5		0.3263	0.3286	0.3286
1.75		0.3794	0.3803	0.3803
2		0.4292	0.4297	0.4297
2.5		0.5192	0.5194	0.5194
3	0.5422	0.5957	0.5958	0.5958
4	0.6870	0.7115	0.7115	0.7115
5	0.7744	0.7887	0.7887	0.7887
7.5	0.8846	0.8905	0.8905	0.8905
10	0.9313	0.9345	0.9345	0.9345
15	0.9682	0.9696	0.9696	0.9696
20	0.9822	0.9830	0.9830	0.9830
40	0.9955	0.9957	0.9957	0.9957
∞	1	1	1	1

Appendix D

Table D1: Readings of current & voltage for the as-cast P3HT thin films as measured in the light.

Thin film sample #	Current (10^{-8}) (A)	Voltage (V)
1	1.00	0.00090
	2.00	0.0039
	3.00	0.0072
	4.00	0.0095
2	**Current (10^{-8}) (A)**	**Voltage (V)**
	1.00	0.0012
	2.00	0.0045
	3.00	0.0089
	4.00	0.013
3	**Current (10^{-8}) (A)**	**Voltage (V)**
	1.00	0.0054
	2.00	0.010
	3.00	0.016
	4.00	0.024
4	**Current (10^{-8}) (A)**	**Voltage (V)**
	1.00	0.0069
	2.00	0.010
	3.00	0.020
	4.00	0.032
5	**Current (10^{-8}) (A)**	**Voltage (V)**
	1.00	0.0096
	2.00	0.018
	3.00	0.029
	4.00	0.043
6	**Current (10^{-8}) (A)**	**Voltage (V)**
	1.00	0.0088
	2.00	0.015
	3.00	0.028
	4.00	0.047
7	**Current (10^{-8}) (A)**	**Voltage (V)**
	1.00	0.012
	2.00	0.015
	3.00	0.025
	4.00	0.035
8	**Current (10^{-8}) (A)**	**Voltage (V)**
	1.00	0.0076
	2.00	0.011
	3.00	0.020
	4.00	0.024

Table D2: Readings of current & voltage for the as-cast P3HT thin films as measured in the dark.

Thin film sample #	Current (10^{-8}) (A)	Voltage (V)
1	1.00	0.0022
	2.00	0.0041
	3.00	0.0077
	4.00	0.010
2	**Current (10^{-8}) (A)**	**Voltage (V)**
	1.00	0.0056
	2.00	0.0088
	3.00	0.0097
	4.00	0.014
3	**Current (10^{-8}) (A)**	**Voltage (V)**
	1.00	0.0062
	2.00	0.0083
	3.00	0.014
	4.00	0.023
4	**Current (10^{-8}) (A)**	**Voltage (V)**
	1.00	0.0096
	2.00	0.016
	3.00	0.021
	4.00	0.030
5	**Current (10^{-8}) (A)**	**Voltage (V)**
	1.00	0.0082
	2.00	0.018
	3.00	0.029
	4.00	0.041
6	**Current (10^{-8}) (A)**	**Voltage (V)**
	1.00	0.010
	2.00	0.014
	3.00	0.030
	4.00	0.039
7	**Current (10^{-8}) (A)**	**Voltage (V)**
	1.00	0.011
	2.00	0.018
	3.00	0.022
	4.00	0.032
8	**Current (10^{-8}) (A)**	**Voltage (V)**
	1.00	0.0096
	2.00	0.014
	3.00	0.017
	4.00	0.020

Table D3: Readings of current & voltage for the annealed P3HT thin films as measured in the light.

Thin film sample #	Current (10^{-8}) (A)	Voltage (V)
1	1.00	0.00040
	2.00	0.0016
	3.00	0.0025
	4.00	0.0039
2	**Current (10^{-8}) (A)**	**Voltage (V)**
	1.00	0.0010
	2.00	0.0021
	3.00	0.0035
	4.00	0.0049
3	**Current (10^{-8}) (A)**	**Voltage (V)**
	1.00	0.00060
	2.00	0.0019
	3.00	0.0042
	4.00	0.0072
4	**Current (10^{-8}) (A)**	**Voltage (V)**
	1.00	0.00090
	2.00	0.0036
	3.00	0.0051
	4.00	0.011
5	**Current (10^{-8}) (A)**	**Voltage (V)**
	1.00	0.0014
	2.00	0.0059
	3.00	0.012
	4.00	0.020
6	**Current (10^{-8}) (A)**	**Voltage (V)**
	1.00	0.0024
	2.00	0.0058
	3.00	0.015
	4.00	0.022
7	**Current (10^{-8}) (A)**	**Voltage (V)**
	1.00	0.0045
	2.00	0.011
	3.00	0.020
	4.00	0.024
8	**Current (10^{-8}) (A)**	**Voltage (V)**
	1.00	0.0039
	2.00	0.0090
	3.00	0.016
	4.00	0.024

Table D4: Readings of current & voltage for the annealed P3HT thin films as measured in the dark.

Thin film sample #	Current (10^{-8}) (A)	Voltage (V)
1	1.00	0.0028
	2.00	0.0048
	3.00	0.0065
	4.00	0.0094
2	**Current (10^{-8}) (A)**	**Voltage (V)**
	1.00	0.0032
	2.00	0.0070
	3.00	0.012
	4.00	0.020
3	**Current (10^{-8}) (A)**	**Voltage (V)**
	1.00	0.0041
	2.00	0.0090
	3.00	0.015
	4.00	0.020
4	**Current (10^{-8}) (A)**	**Voltage (V)**
	1.00	0.0069
	2.00	0.012
	3.00	0.020
	4.00	0.026
5	**Current (10^{-8}) (A)**	**Voltage (V)**
	1.00	0.0067
	2.00	0.011
	3.00	0.020
	4.00	0.027
6	**Current (10^{-8}) (A)**	**Voltage (V)**
	1.00	0.0070
	2.00	0.010
	3.00	0.020
	4.00	0.028
7	**Current (10^{-8}) (A)**	**Voltage (V)**
	1.00	0.0058
	2.00	0.013
	3.00	0.018
	4.00	0.029
8	**Current (10^{-8}) (A)**	**Voltage (V)**
	1.00	0.0059
	2.00	0.0088
	3.00	0.013
	4.00	0.018

Appendix E

Table E1: Linear regression for the calculated $R_{\square}$ and estimated thickness.

```
                            OLS Regression Results
==============================================================================
Dep. Variable:                      y   R-squared (uncentered):                   0.932
Model:                            OLS   Adj. R-squared (uncentered):              0.923
Method:                 Least Squares   F-statistic:                              96.35
Date:                Thu, 08 Jun 2023   Prob (F-statistic):                    2.42e-05
Time:                        13:48:44   Log-Likelihood:                         -59.033
No. Observations:                   8   AIC:                                      120.1
Df Residuals:                       7   BIC:                                      120.1
Df Model:                           1
Covariance Type:            nonrobust
==============================================================================
                 coef    std err          t      P>|t|      [0.025      0.975]
------------------------------------------------------------------------------
x1           438.5227     44.675      9.816      0.000     332.882     544.163
==============================================================================
Omnibus:                        0.783   Durbin-Watson:                   1.525
Prob(Omnibus):                  0.676   Jarque-Bera (JB):                0.638
Skew:                           0.486   Prob(JB):                        0.727
Kurtosis:                       2.015   Cond. No.                         1.00
==============================================================================

Notes:
[1] R² is computed without centering (uncentered) since the model does not contain a constant.
[2] Standard Errors assume that the covariance matrix of the errors is correctly specified.
C:\\Users\\Basho\\AppData\\Local\\Programs\\Python\\Python310\\lib\\site-packages\\scipy\\stats\\_stats_py.py:1736: UserWarning: kurtosistest only valid for n>=20 ... continuing anyway, n=8
  warnings.warn("kurtosistest only valid for n>=20 ... continuing "
                            OLS Regression Results
==============================================================================
Dep. Variable:                      y   R-squared (uncentered):                   0.920
Model:                            OLS   Adj. R-squared (uncentered):              0.909
Method:                 Least Squares   F-statistic:                              80.70
Date:                Thu, 08 Jun 2023   Prob (F-statistic):                    4.32e-05
Time:                        13:48:44   Log-Likelihood:                         -59.689
No. Observations:                   8   AIC:                                      121.4
```

Page 1 of 22

```
Df Residuals:                     7   BIC:                            121.5
Df Model:                         1
Covariance Type:            nonrobust
==============================================================================
                 coef    std err          t      P>|t|      [0.025      0.975]
------------------------------------------------------------------------------
x1           544.4774     60.610      8.983      0.000     401.158     687.797
==============================================================================
Omnibus:                        3.107   Durbin-Watson:                   1.219
Prob(Omnibus):                  0.211   Jarque-Bera (JB):                0.468
Skew:                           0.540   Prob(JB):                        0.791
Kurtosis:                       3.490   Cond. No.                         1.00
==============================================================================

Notes:
[1] R² is computed without centering (uncentered) since the model does not contain a constant.
[2] Standard Errors assume that the covariance matrix of the errors is correctly specified.
C:\Users\Basho\AppData\Local\Programs\Python\Python310\lib\site-packages\scipy\stats\_stats_py.py:1736: UserWarning: kurtosistest only valid for n>=20 ... continuing anyway, n=8
  warnings.warn("kurtosistest only valid for n>=20 ... continuing "
                            OLS Regression Results
==============================================================================
Dep. Variable:                      y   R-squared (uncentered):                   0.934
Model:                            OLS   Adj. R-squared (uncentered):              0.925
Method:                 Least Squares   F-statistic:                              99.66
Date:                Thu, 08 Jun 2023   Prob (F-statistic):                    2.16e-05
Time:                        13:48:44   Log-Likelihood:                         -58.906
No. Observations:                   8   AIC:                                      119.8
Df Residuals:                       7   BIC:                                      119.9
Df Model:                           1
Covariance Type:            nonrobust
==============================================================================
                 coef    std err          t      P>|t|      [0.025      0.975]
------------------------------------------------------------------------------
x1           475.0485     47.585      9.983      0.000     362.528     587.569
==============================================================================
Omnibus:                        4.355   Durbin-Watson:                   0.735
Prob(Omnibus):                  0.113   Jarque-Bera (JB):                1.181
Skew:                           0.921   Prob(JB):                        0.554
Kurtosis:                       3.386   Cond. No.                         1.00
==============================================================================

```

```
                            OLS Regression Results
==============================================================================
Dep. Variable:                      y   R-squared (uncentered):                   0.889
Model:                            OLS   Adj. R-squared (uncentered):              0.873
Method:                 Least Squares   F-statistic:                              55.92
Date:                Thu, 08 Jun 2023   Prob (F-statistic):                    0.000140
Time:                        13:48:44   Log-Likelihood:                         -61.017
No. Observations:                   8   AIC:                                      124.0
Df Residuals:                       7   BIC:                                      124.1
Df Model:                           1
Covariance Type:            nonrobust
==============================================================================
                 coef    std err          t      P>|t|      [0.025      0.975]
------------------------------------------------------------------------------
x1           411.8352     55.072      7.478      0.000     281.611     542.060
==============================================================================
Omnibus:                        5.511   Durbin-Watson:                   0.683
Prob(Omnibus):                  0.064   Jarque-Bera (JB):                1.728
Skew:                           1.120   Prob(JB):                        0.421
Kurtosis:                       3.414   Cond. No.                         1.00
==============================================================================

Notes:
[1] R² is computed without centering (uncentered) since the model does not contain a constant.
[2] Standard Errors assume that the covariance matrix of the errors is correctly specified.
                            OLS Regression Results
==============================================================================
Dep. Variable:                      y   R-squared (uncentered):                   0.318
Model:                            OLS   Adj. R-squared (uncentered):              0.221
Method:                 Least Squares   F-statistic:                              3.271
Date:                Thu, 08 Jun 2023   Prob (F-statistic):                      0.113
Time:                        13:48:44   Log-Likelihood:                          45.138
No. Observations:                   8   AIC:                                    -88.28
Df Residuals:                       7   BIC:                                    -88.20
Df Model:                           1
Covariance Type:            nonrobust
```

```
121 ==============================================================================
    ====================
122                 coef    std err          t      P>|t|      [0.025      0.975]
123 ------------------------------------------------------------------------------
124 x1             0.0002   9.89e-05      1.808      0.113    -5.5e-05       0.000
125 ==============================================================================
    ====================
126 Omnibus:                        2.457   Durbin-Watson:                   0.223
127 Prob(Omnibus):                  0.293   Jarque-Bera (JB):                1.169
128 Skew:                           0.905   Prob(JB):                        0.557
129 Kurtosis:                       2.517   Cond. No.                         1.00
130 ==============================================================================
    ==================
131
132 Notes:
133 [1] R² is computed without centering (uncentered) since the model does not contain a
    constant.
134 [2] Standard Errors assume that the covariance matrix of the errors is correctly
    specified.
135 C:\Users\Basho\AppData\Local\Programs\Python\Python310\lib\site-packages\scipy\
    stats\_stats_py.py:1736: UserWarning: kurtosistest only valid for n>=20 ... continuing
     anyway, n=8
136   warnings.warn("kurtosistest only valid for n>=20 ... continuing "
137 C:\Users\Basho\AppData\Local\Programs\Python\Python310\lib\site-packages\scipy\
    stats\_stats_py.py:1736: UserWarning: kurtosistest only valid for n>=20 ... continuing
     anyway, n=8
138   warnings.warn("kurtosistest only valid for n>=20 ... continuing "
139 C:\Users\Basho\AppData\Local\Programs\Python\Python310\lib\site-packages\scipy\
    stats\_stats_py.py:1736: UserWarning: kurtosistest only valid for n>=20 ... continuing
     anyway, n=8
140   warnings.warn("kurtosistest only valid for n>=20 ... continuing "
141                             OLS Regression Results
142 ==============================================================================
    ==============================
143 Dep. Variable:                    y   R-squared (uncentered):                   0.430
144 Model:                          OLS   Adj. R-squared (uncentered):              0.348
145 Method:               Least Squares   F-statistic:                             5.278
146 Date:              Thu, 08 Jun 2023   Prob (F-statistic):                      0.0552
147 Time:                      13:48:44   Log-Likelihood:                         45.852
148 No. Observations:                 8   AIC:                                    -89.70
149 Df Residuals:                     7   BIC:                                    -89.62
150 Df Model:                         1
151 Covariance Type:            nonrobust
152 ==============================================================================
    ==================
153                 coef    std err          t      P>|t|      [0.025      0.975]
154 ------------------------------------------------------------------------------
155 x1             0.0003      0.000      2.297      0.055    -7.6e-06       0.001
156 ==============================================================================
    ==================
157 Omnibus:                        2.765   Durbin-Watson:                   0.272
158 Prob(Omnibus):                  0.251   Jarque-Bera (JB):                1.272
```

```
Skew:                          0.953   Prob(JB):                     0.529
Kurtosis:                      2.570   Cond. No.                      1.00
==============================================================================
                  OLS Regression Results
==============================================================================
Dep. Variable:                    y   R-squared (uncentered):                0.443
Model:                          OLS   Adj. R-squared (uncentered):           0.364
Method:               Least Squares   F-statistic:                           5.574
Date:              Thu, 08 Jun 2023   Prob (F-statistic):                  0.0503
Time:                      13:48:44   Log-Likelihood:                       45.947
No. Observations:                 8   AIC:                                 -89.89
Df Residuals:                     7   BIC:                                 -89.82
Df Model:                         1
Covariance Type:          nonrobust
==============================================================================
                 coef    std err          t      P>|t|      [0.025      0.975]
------------------------------------------------------------------------------
x1             0.0002   9.67e-05      2.361      0.050    -3.5e-07       0.000
==============================================================================
Omnibus:                        2.836   Durbin-Watson:                   0.240
Prob(Omnibus):                  0.242   Jarque-Bera (JB):                1.302
Skew:                          0.965   Prob(JB):                        0.522
Kurtosis:                      2.576   Cond. No.                         1.00
==============================================================================

Notes:
[1] R² is computed without centering (uncentered) since the model does not contain a constant.
[2] Standard Errors assume that the covariance matrix of the errors is correctly specified.
C:\Users\Basho\AppData\Local\Programs\Python\Python310\lib\site-packages\scipy\stats\_stats_py.py:1736: UserWarning: kurtosistest only valid for n>=20 ... continuing anyway, n=8
  warnings.warn("kurtosistest only valid for n>=20 ... continuing "
C:\Users\Basho\AppData\Local\Programs\Python\Python310\lib\site-packages\scipy\stats\_stats_py.py:1736: UserWarning: kurtosistest only valid for n>=20 ... continuing anyway, n=8
  warnings.warn("kurtosistest only valid for n>=20 ... continuing "
                  OLS Regression Results
==============================================================================
```

```
Dep. Variable:                    y   R-squared (uncentered):                   0.432
Model:                          OLS   Adj. R-squared (uncentered):              0.351
Method:               Least Squares   F-statistic:                              5.330
Date:              Thu, 08 Jun 2023   Prob (F-statistic):                      0.0543
Time:                      13:48:44   Log-Likelihood:                          45.869
No. Observations:                 8   AIC:                                     -89.74
Df Residuals:                     7   BIC:                                     -89.66
Df Model:                         1
Covariance Type:          nonrobust
==============================================================================
                 coef    std err          t      P>|t|      [0.025      0.975]
------------------------------------------------------------------------------
x1             0.0002   8.68e-05      2.309      0.054   -4.85e-06       0.000
==============================================================================
Omnibus:                        2.963   Durban-Watson:                   0.260
Prob(Omnibus):                  0.227   Jarque-Bera (JB):                1.282
Skew:                           0.966   Prob(JB):                        0.527
Kurtosis:                       2.660   Cond. No.                         1.00
==============================================================================

Notes:
[1] R² is computed without centering (uncentered) since the model does not contain a constant.
[2] Standard Errors assume that the covariance matrix of the errors is correctly specified.
                            OLS Regression Results
==============================================================================
Dep. Variable:                    y   R-squared (uncentered):                   0.966
Model:                          OLS   Adj. R-squared (uncentered):              0.961
Method:               Least Squares   F-statistic:                              197.9
Date:              Thu, 08 Jun 2023   Prob (F-statistic):                    2.18e-06
Time:                      13:48:44   Log-Likelihood:                         -56.296
No. Observations:                 8   AIC:                                      114.6
Df Residuals:                     7   BIC:                                      114.7
Df Model:                         1
Covariance Type:          nonrobust
==============================================================================
                 coef    std err          t      P>|t|      [0.025      0.975]
------------------------------------------------------------------------------
x1           405.0685     28.797     14.067      0.000     336.975     473.162
==============================================================================
Omnibus:                        1.451   Durban-Watson:                   1.232
Prob(Omnibus):                  0.484   Jarque-Bera (JB):                0.213
Skew:                           0.399   Prob(JB):                        0.899
Kurtosis:                       2.980   Cond. No.                         1.00
==============================================================================
```

```
                            OLS Regression Results
==============================================================================
Dep. Variable:                      y   R-squared (uncentered):                   0.943
Model:                            OLS   Adj. R-squared (uncentered):              0.934
Method:                 Least Squares   F-statistic:                              115.0
Date:                Thu, 08 Jun 2023   Prob (F-statistic):                    1.35e-05
Time:                        13:48:44   Log-Likelihood:                         -58.370
No. Observations:                   8   AIC:                                      118.7
Df Residuals:                       7   BIC:                                      118.8
Df Model:                           1
Covariance Type:            nonrobust
==============================================================================
                 coef    std err          t      P>|t|      [0.025      0.975]
------------------------------------------------------------------------------
x1           492.1333     45.898     10.722      0.000     383.602     600.664
==============================================================================
Omnibus:                        0.712   Durbin-Watson:                   1.257
Prob(Omnibus):                  0.700   Jarque-Bera (JB):                0.269
Skew:                           0.397   Prob(JB):                        0.874
Kurtosis:                       2.579   Cond. No.                         1.00
==============================================================================

Notes:
[1] R² is computed without centering (uncentered) since the model does not contain a constant.
[2] Standard Errors assume that the covariance matrix of the errors is correctly specified.
C:\Users\Basho\AppData\Local\Programs\Python\Python310\lib\site-packages\scipy\stats\_stats_py.py:1736: UserWarning: kurtosistest only valid for n>=20 ... continuing anyway, n=8
  warnings.warn("kurtosistest only valid for n>=20 ... continuing "
                            OLS Regression Results
==============================================================================
Dep. Variable:                      y   R-squared (uncentered):                   0.905
Model:                            OLS   Adj. R-squared (uncentered):              0.892
Method:                 Least Squares   F-statistic:                              66.79
```

```
Date:                Thu, 08 Jun 2023   Prob (F-statistic):                7.95e-05
Time:                        13:48:44   Log-Likelihood:                    -60.380
No. Observations:                   8   AIC:                                122.8
Df Residuals:                       7   BIC:                                122.8
Df Model:                           1
Covariance Type:            nonrobust
==============================================================================
                 coef    std err          t      P>|t|      [0.025      0.975]
------------------------------------------------------------------------------
x1           476.5671     58.311      8.173      0.000     338.682     614.452
==============================================================================
Omnibus:                        3.679   Durbin-Watson:                   0.683
Prob(Omnibus):                  0.159   Jarque-Bera (JB):                1.209
Skew:                           0.952   Prob(JB):                        0.546
Kurtosis:                       3.056   Cond. No.                         1.00
==============================================================================

Notes:
[1] R² is computed without centering (uncentered) since the model does not contain a constant.
[2] Standard Errors assume that the covariance matrix of the errors is correctly specified.
C:\Users\Basho\AppData\Local\Programs\Python\Python310\lib\site-packages\scipy\stats\_stats_py.py:1736: UserWarning: kurtosistest only valid for n>=20 ... continuing anyway, n=8
  warnings.warn("kurtosistest only valid for n>=20 ... continuing "
                            OLS Regression Results
==============================================================================
Dep. Variable:                      y   R-squared (uncentered):                   0.878
Model:                            OLS   Adj. R-squared (uncentered):              0.861
Method:                 Least Squares   F-statistic:                              50.42
Date:                Thu, 08 Jun 2023   Prob (F-statistic):                    0.000194
Time:                        13:48:45   Log-Likelihood:                         -61.383
No. Observations:                   8   AIC:                                      124.8
Df Residuals:                       7   BIC:                                      124.8
Df Model:                           1
Covariance Type:            nonrobust
==============================================================================
                 coef    std err          t      P>|t|      [0.025      0.975]
------------------------------------------------------------------------------
x1           455.3715     64.129      7.101      0.000     303.731     607.012
==============================================================================
Omnibus:                        7.289   Durbin-Watson:                   0.628
Prob(Omnibus):                  0.026   Jarque-Bera (JB):                2.276
Skew:                           1.250   Prob(JB):                        0.321
Kurtosis:                       3.757   Cond. No.                         1.00
```

```
                            OLS Regression Results
==============================================================================
Dep. Variable:                      y   R-squared (uncentered):                   0.464
Model:                            OLS   Adj. R-squared (uncentered):              0.387
Method:                 Least Squares   F-statistic:                              6.051
Date:                Thu, 08 Jun 2023   Prob (F-statistic):                      0.0435
Time:                        13:48:45   Log-Likelihood:                          46.096
No. Observations:                   8   AIC:                                     -90.19
Df Residuals:                       7   BIC:                                     -90.11
Df Model:                           1
Covariance Type:            nonrobust
==============================================================================
                 coef    std err          t      P>|t|      [0.025      0.975]
------------------------------------------------------------------------------
x1             0.0002   7.96e-05      2.460      0.043    7.58e-06       0.000
==============================================================================
Omnibus:                        4.574   Durbin-Watson:                   0.301
Prob(Omnibus):                  0.102   Jarque-Bera (JB):                1.653
Skew:                           1.113   Prob(JB):                        0.438
Kurtosis:                       3.059   Cond. No.                         1.00
==============================================================================

Notes:
[1] R² is computed without centering (uncentered) since the model does not contain a constant.
[2] Standard Errors assume that the covariance matrix of the errors is correctly specified.
C:\Users\Basho\AppData\Local\Programs\Python\Python310\lib\site-packages\scipy\stats\_stats_py.py:1736: UserWarning: kurtosistest only valid for n>=20 ... continuing anyway, n=8
  warnings.warn("kurtosistest only valid for n>=20 ... continuing "
C:\Users\Basho\AppData\Local\Programs\Python\Python310\lib\site-packages\scipy\stats\_stats_py.py:1736: UserWarning: kurtosistest only valid for n>=20 ... continuing anyway, n=8
  warnings.warn("kurtosistest only valid for n>=20 ... continuing "
                            OLS Regression Results
```

```
358 ==============================================================================
    ==============================
359 Dep. Variable:                      y   R-squared (uncentered):                   0.465
360 Model:                            OLS   Adj. R-squared (uncentered):              0.388
361 Method:                 Least Squares   F-statistic:                              6.075
362 Date:                Thu, 08 Jun 2023   Prob (F-statistic):                       0.0432
363 Time:                        13:48:45   Log-Likelihood:                          46.104
364 No. Observations:                   8   AIC:                                     -90.21
365 Df Residuals:                       7   BIC:                                     -90.13
366 Df Model:                           1
367 Covariance Type:            nonrobust
368 ==============================================================================
    ==================
369                  coef    std err          t      P>|t|      [0.025      0.975]
370 ------------------------------------------------------------------------------
371 x1             0.0002   9.78e-05      2.465      0.043     9.8e-06       0.000
372 ==============================================================================
    ==================
373 Omnibus:                       3.883   Durbin-Watson:                   0.310
374 Prob(Omnibus):                  0.144   Jarque-Bera (JB):                1.522
375 Skew:                          1.066   Prob(JB):                        0.467
376 Kurtosis:                      2.866   Cond. No.                         1.00
377 ==============================================================================
    ==================
378
379 Notes:
380 [1] R² is computed without centering (uncentered) since the model does not contain a
    constant.
381 [2] Standard Errors assume that the covariance matrix of the errors is correctly
    specified.
382                             OLS Regression Results
383 ==============================================================================
    ==============================
384 Dep. Variable:                      y   R-squared (uncentered):                   0.456
385 Model:                            OLS   Adj. R-squared (uncentered):              0.379
386 Method:                 Least Squares   F-statistic:                              5.874
387 Date:                Thu, 08 Jun 2023   Prob (F-statistic):                       0.0459
388 Time:                        13:48:45   Log-Likelihood:                          46.042
389 No. Observations:                   8   AIC:                                     -90.08
390 Df Residuals:                       7   BIC:                                     -90.00
391 Df Model:                           1
392 Covariance Type:            nonrobust
393 ==============================================================================
    ==================
394                  coef    std err          t      P>|t|      [0.025      0.975]
395 ------------------------------------------------------------------------------
396 x1             0.0002   9.74e-05      2.424      0.046    5.74e-06       0.000
397 ==============================================================================
    ==================
398 Omnibus:                       2.612   Durbin-Watson:                   0.255
399 Prob(Omnibus):                  0.271   Jarque-Bera (JB):                1.210
400 Skew:                          0.926   Prob(JB):                        0.546
```

```
Kurtosis:                       2.556   Cond. No.                         1.00
==============================================================================
                                                                              

Notes:
[1] R² is computed without centering (uncentered) since the model does not contain a constant.
[2] Standard Errors assume that the covariance matrix of the errors is correctly specified.
C:\Users\Basho\AppData\Local\Programs\Python\Python310\lib\site-packages\scipy\stats\_stats_py.py:1736: UserWarning: kurtosistest only valid for n>=20 ... continuing anyway, n=8
  warnings.warn("kurtosistest only valid for n>=20 ... continuing "
C:\Users\Basho\AppData\Local\Programs\Python\Python310\lib\site-packages\scipy\stats\_stats_py.py:1736: UserWarning: kurtosistest only valid for n>=20 ... continuing anyway, n=8
  warnings.warn("kurtosistest only valid for n>=20 ... continuing "
                            OLS Regression Results
==============================================================================
Dep. Variable:                      y   R-squared (uncentered):                   0.466
Model:                            OLS   Adj. R-squared (uncentered):              0.390
Method:                 Least Squares   F-statistic:                              6.107
Date:                Thu, 08 Jun 2023   Prob (F-statistic):                      0.0428
Time:                        13:48:45   Log-Likelihood:                         46.113
No. Observations:                   8   AIC:                                    -90.23
Df Residuals:                       7   BIC:                                    -90.15
Df Model:                           1                                         
Covariance Type:            nonrobust                                         
==============================================================================
                 coef    std err          t      P>|t|      [0.025      0.975]
------------------------------------------------------------------------------
x1             0.0002   9.36e-05      2.471      0.043    9.98e-06       0.000
==============================================================================
Omnibus:                        3.257   Durbin-Watson:                   0.278
Prob(Omnibus):                  0.196   Jarque-Bera (JB):                1.369
Skew:                           1.003   Prob(JB):                        0.504
Kurtosis:                       2.718   Cond. No.                         1.00
==============================================================================

Notes:
[1] R² is computed without centering (uncentered) since the model does not contain a constant.
[2] Standard Errors assume that the covariance matrix of the errors is correctly specified.
                            OLS Regression Results
==============================================================================
Dep. Variable:                      y   R-squared (uncentered):                   0.934
```

```
Model:                            OLS   Adj. R-squared (uncentered):              0.924
Method:                 Least Squares   F-statistic:                              98.76
Date:                Thu, 08 Jun 2023   Prob (F-statistic):                    2.23e-05
Time:                        13:48:45   Log-Likelihood:                         -58.940
No. Observations:                   8   AIC:                                      119.9
Df Residuals:                       7   BIC:                                      120.0
Df Model:                           1
Covariance Type:            nonrobust
===============================================================================
                 coef    std err          t      P>|t|      [0.025      0.975]
-------------------------------------------------------------------------------
x1           592.7662     59.646      9.938      0.000     451.726     733.807
===============================================================================
Omnibus:                        1.379   Durbin-Watson:                   0.627
Prob(Omnibus):                  0.502   Jarque-Bera (JB):                0.724
Skew:                           0.678   Prob(JB):                        0.696
Kurtosis:                       2.422   Cond. No.                         1.00
===============================================================================

Notes:
[1] R² is computed without centering (uncentered) since the model does not contain a constant.
[2] Standard Errors assume that the covariance matrix of the errors is correctly specified.
C:\Users\Basho\AppData\Local\Programs\Python\Python310\lib\site-packages\scipy\stats\_stats_py.py:1736: UserWarning: kurtosistest only valid for n>=20 ... continuing anyway, n=8
  warnings.warn("kurtosistest only valid for n>=20 ... continuing "
C:\Users\Basho\AppData\Local\Programs\Python\Python310\lib\site-packages\scipy\stats\_stats_py.py:1736: UserWarning: kurtosistest only valid for n>=20 ... continuing anyway, n=8
  warnings.warn("kurtosistest only valid for n>=20 ... continuing "
C:\Users\Basho\AppData\Local\Programs\Python\Python310\lib\site-packages\scipy\stats\_stats_py.py:1736: UserWarning: kurtosistest only valid for n>=20 ... continuing anyway, n=8
  warnings.warn("kurtosistest only valid for n>=20 ... continuing "
                                 OLS Regression Results
=======================================================================================
Dep. Variable:                      y   R-squared (uncentered):                   0.915
Model:                            OLS   Adj. R-squared (uncentered):              0.903
Method:                 Least Squares   F-statistic:                              75.33
Date:                Thu, 08 Jun 2023   Prob (F-statistic):                    5.40e-05
Time:                        13:48:45   Log-Likelihood:                         -59.942
No. Observations:                   8   AIC:                                      121.9
Df Residuals:                       7   BIC:                                      122.0
Df Model:                           1
Covariance Type:            nonrobust
=======================================================================================
```

```
==============
                 coef    std err          t      P>|t|      [0.025      0.975]
------------------------------------------------------------------------------
x1           664.0412     76.510      8.679      0.000     483.124     844.958
==============================================================================
Omnibus:                        5.610   Durbin-Watson:                   0.762
Prob(Omnibus):                  0.061   Jarque-Bera (JB):                1.728
Skew:                           1.115   Prob(JB):                        0.421
Kurtosis:                       3.460   Cond. No.                         1.00
==============================================================================

Notes:
[1] R² is computed without centering (uncentered) since the model does not contain a constant.
[2] Standard Errors assume that the covariance matrix of the errors is correctly specified.
                            OLS Regression Results
==============================================================================
Dep. Variable:                      y   R-squared (uncentered):                   0.886
Model:                            OLS   Adj. R-squared (uncentered):              0.870
Method:                 Least Squares   F-statistic:                              54.41
Date:                Thu, 08 Jun 2023   Prob (F-statistic):                    0.000153
Time:                        13:48:45   Log-Likelihood:                         -61.115
No. Observations:                   8   AIC:                                      124.2
Df Residuals:                       7   BIC:                                      124.3
Df Model:                           1
Covariance Type:            nonrobust
==============
                 coef    std err          t      P>|t|      [0.025      0.975]
------------------------------------------------------------------------------
x1           593.1638     80.418      7.376      0.000     403.005     783.323
==============================================================================
Omnibus:                        6.906   Durbin-Watson:                   0.459
Prob(Omnibus):                  0.032   Jarque-Bera (JB):                2.328
Skew:                           1.296   Prob(JB):                        0.312
Kurtosis:                       3.517   Cond. No.                         1.00
==============================================================================

Notes:
[1] R² is computed without centering (uncentered) since the model does not contain a constant.
[2] Standard Errors assume that the covariance matrix of the errors is correctly specified.
                            OLS Regression Results
==============================================================================
```

```
                            OLS Regression Results
==============================================================================
Dep. Variable:                      y   R-squared (uncentered):                   0.903
Model:                            OLS   Adj. R-squared (uncentered):              0.889
Method:                 Least Squares   F-statistic:                              65.32
Date:                Thu, 08 Jun 2023   Prob (F-statistic):                    8.54e-05
Time:                        13:48:45   Log-Likelihood:                         -60.461
No. Observations:                   8   AIC:                                      122.9
Df Residuals:                       7   BIC:                                      123.0
Df Model:                           1
Covariance Type:            nonrobust
==============================================================================
                 coef    std err          t      P>|t|      [0.025      0.975]
------------------------------------------------------------------------------
x1           563.3609     69.707      8.082      0.000     398.530     728.192
==============================================================================
Omnibus:                       11.424   Durbin-Watson:                   0.671
Prob(Omnibus):                  0.003   Jarque-Bera (JB):                3.893
Skew:                           1.558   Prob(JB):                        0.143
Kurtosis:                       4.405   Cond. No.                         1.00
==============================================================================

Notes:
[1] R² is computed without centering (uncentered) since the model does not contain a constant.
[2] Standard Errors assume that the covariance matrix of the errors is correctly specified.
                            OLS Regression Results
==============================================================================
Dep. Variable:                      y   R-squared (uncentered):                   0.530
Model:                            OLS   Adj. R-squared (uncentered):              0.463
Method:                 Least Squares   F-statistic:                              7.886
Date:                Thu, 08 Jun 2023   Prob (F-statistic):                     0.0262
Time:                        13:48:45   Log-Likelihood:                          46.623
No. Observations:                   8   AIC:                                     -91.25
Df Residuals:                       7   BIC:                                     -91.17
Df Model:                           1
Covariance Type:            nonrobust
==============================================================================
                 coef    std err          t      P>|t|      [0.025      0.975]
------------------------------------------------------------------------------
x1             0.0003      0.000      2.808      0.026     4.92e-05       0.001
==============================================================================
Omnibus:                        3.313   Durbin-Watson:                   0.273
Prob(Omnibus):                  0.191   Jarque-Bera (JB):                1.471
Skew:                           1.035   Prob(JB):                        0.479
Kurtosis:                       2.646   Cond. No.                         1.00
==============================================================================
```